Title

Postsynaptic Serine Racemase Regulates NMDA Receptor Function

Journal

Journal of Neuroscience, 40(50)

ISSN

0270-6474

Authors

Wong, Jonathan M
Folorunso, Oluwarotimi O
Barragan, Eden V
et al.

Publication Date

2020-12-09

DOI

10.1523/jneurosci.1525-20.2020

Peer reviewed

Postsynaptic serine racemase regulates NMDA receptor function

Abbreviated Title: Postsynaptic serine racemase regulates NMDARs

Jonathan M. Wong[1,2,*], Oluwarotimi O. Folorunso[3,4,*], Eden V. Barragan[1,2], Cristina Berciu[3], Theresa L. Harvey[4], Joseph T. Coyle[3], Darrick T. Balu[3,4**], and John A. Gray[1,5**]

(1) Center for Neuroscience, University of California Davis, Davis, CA 95616
(2) Neuroscience Graduate Group, University of California Davis, Davis, CA 95616
(3) Department of Psychiatry, Harvard Medical School, Boston, MA 02115
(4) Translational Psychiatry Laboratory, McLean Hospital, Belmont, MA 02478
(5) Department of Neurology, University of California Davis, Davis, CA 95616

*these authors contributed equally
**corresponding authors

Corresponding Authors:
John A. Gray: john.gray@ucdavis.edu
Darrick T. Balu: dbalu@mclean.harvard.edu

Number of Pages: 37
Number of Figures: 8
Number of Words: Abstract (210), Introduction (463), Discussion (1500)

Conflict of interest: JTC reports consulting with Concert Pharm and holding a patent on D-serine for the treatment of serious mental illness, which is owned by Massachusetts General Hospital. DTB served as a consultant for LifeSci Capital and received research support from Takeda Pharmaceuticals. All other authors declare no competing financial interests.

Acknowledgements: This work was supported by: Jeane B. Kempner Postdoctoral Fellowship Award and McLean Hospital Presidential Award (OOF); T32MH082174 (EB); Whitehall Foundation #2018-05-107 (DTB); BrightFocus Foundation A2019034S (DTB); R03AG063201 (DTB); a subcontract of R01NS098740 (DTB); US-Israel Binational Science Foundation grant (2019021; DTB); R01MH05190 (JTC); R21MH116315 (JAG); and R01MH117130 (JAG). We would like to thank Haley Martin, Zaiyang "Sunny" Zhang, and Casey Sawyer for their assistance in mouse breeding and genotyping.

Abstract

D-serine is the primary NMDA receptor (NMDAR) co-agonist at mature forebrain synapses and is synthesized by the enzyme serine racemase (SR). However, our understanding of the mechanisms regulating the availability of synaptic D-serine remains limited. Though early studies suggested D-serine is synthesized and released from astrocytes, more recent studies have demonstrated a predominantly neuronal localization of SR. More specifically, recent work intriguingly suggests that SR may be found at the postsynaptic density, yet the functional implications of postsynaptic SR on synaptic transmission are not yet known. Here, we show an age-dependent dendritic and postsynaptic localization of SR and D-serine by immunohistochemistry and electron microscopy in mouse CA1 pyramidal neurons. In addition, using a single-neuron genetic approach in SR conditional knockout mice from both sexes, we demonstrate a cell-autonomous role for SR in regulating synaptic NMDAR function at Schaffer collateral (CA3)-CA1 synapses. Importantly, single-neuron genetic deletion of SR resulted in the elimination of LTP at one month of age, which could be rescued by exogenous D-serine. Interestingly, there was a restoration of LTP by two months of age that was associated with an upregulation of synaptic GluN2B. Our findings support a cell-autonomous role for postsynaptic neuronal SR in regulating synaptic NMDAR function and suggests a possible autocrine mode of D-serine action.

Significance Statement

NMDA receptors (NMDARs) are key regulators of neurodevelopment and synaptic plasticity and are unique in their requirement for binding of a co-agonist, which is D-serine at most forebrain synapses. However, our understanding of the

mechanisms regulating synaptic D-serine availability remains limited. D-serine is synthesized in the brain by the neuronal enzyme serine racemase (SR). Here, we show dendritic and postsynaptic localization of SR and D-serine in CA1 pyramidal neurons. In addition, using single-neuron genetic deletion of SR, we establish a role of postsynaptic SR in regulating NMDAR function. These results support an autocrine mode of D-serine action at synapses.

Introduction

NMDA receptors (NMDARs) are glutamate receptors, which have a property unique among ion channels: they require a co-agonist for channel opening (Johnson and Ascher, 1987; Kleckner and Dingledine, 1988). In addition to glutamate binding to the GluN2 subunits, either glycine or D-serine must bind to the GluN1 subunits. D-serine is the primary co-agonist at most mature forebrain synapses, including the Schaffer collateral-CA1 synapse in the hippocampus (Mothet et al., 2000; Papouin et al., 2012; Le Bail et al., 2015) and is synthesized in the brain by the enzyme serine racemase (SR), which converts L-serine to D-serine (Wolosker et al., 1999). However, our understanding of the mechanisms regulating the availability of synaptic D-serine remains limited.

Early studies suggested that D-serine is synthesized and released by astrocytes leading to the labeling of D-serine as a "gliotransmitter" (Schell et al., 1995; Schell et al., 1997; Wolosker et al., 1999; Panatier et al., 2006). However, more recent studies have demonstrated a predominantly neuronal localization (Wolosker et al., 2016). Indeed, germline SR knock-out (KO) mice have been used to validate SR antibody specificity, identifying a preferential expression of SR in neurons in rodent and human brains (Kartvelishvily et al., 2006; Miya et al., 2008; Basu et al., 2009; Ding et al., 2011; Balu et

al., 2014; Balu et al., 2018). This neuronal localization of SR was further supported by *in situ* hybridization (Yoshikawa et al., 2007) and in transgenic mice where the SR coding region was replaced by GFP (Ehmsen et al., 2013). Convincingly, genetic deletion of SR from pyramidal neurons, but not from astrocytes, leads to reduction of brain D-serine concentration (Benneyworth et al., 2012; Ishiwata et al., 2015), and impairment of long term potentiation (LTP) at CA3-CA1 synapses (Benneyworth et al., 2012; Perez et al., 2017). Furthermore, biochemical evidence from adult rat brain demonstrated the presence of SR in synaptosomes (Balan et al., 2009), and SR has been found to co-localize and co-immunoprecipitate with postsynaptic density protein 95 (PSD-95) in cortical neuronal cultures, supporting a postsynaptic localization of SR (Ma et al., 2014; Lin et al., 2016). However, the functional implications of postsynaptic SR on synaptic transmission are not known.

Here, we demonstrate dendritic and postsynaptic localization of SR and D-serine by immunohistochemistry and electron microscopy in hippocampal CA1 neurons. In addition, using a single-neuron genetic approach in SR conditional knockout mice, we demonstrate a cell-autonomous role for SR in regulating synaptic NMDAR function. Importantly, single-neuron genetic deletion of SR resulted in the elimination of CA3-CA1 LTP at one month of age, which was rescued by exogenous D-serine administration. Interestingly, LTP was restored by two months with a concomitant upregulation of synaptic GluN2B. This evidence supports a cell-autonomous role for postsynaptic neuronal SR in regulating synaptic function and suggests a possible autocrine mode of D-serine action.

Materials and Methods

Animals

The floxed (fl) SR construct was generated as previously described (Basu et al., 2009; Benneyworth et al., 2012). In this construct, the first coding exon (exon 3) is flanked by loxP sites, which results in excision of the intervening sequence upon exposure to Cre recombinase. These *Srr*$^{fl/fl}$ mice are maintained on a C57B/L6J background. WT and constitutive SR knockout (SR-/-) mice were produced by breeding SR heterozygous (SR+/-) parents. Mice were grouped housed in polycarbonate cages and maintained on a 12-hour light/dark cycle. Mice of both sexes were used. Animals were given access to food and water *ad libitum*. The University of California Davis and McLean Hospital Institutional Animal Care and Use Committee approved all animal procedures.

Immunofluorescence

Postnatal day 16 (P16) and two month-old wild-type or SR-/- C57B/L6 mice were deeply anesthetized, briefly intracardially perfused with cold PBS (0.5M phosphate buffer, NaCl, pH 7.4), followed by 4% paraformaldehyde (Electron Microscopy Sciences; EMS) and then in 30% sucrose/PBS at 4°C. Brains were sectioned at 30 µm using a Leica SM 2010R Microtome or Microme HM 505E Cryostat and stored in a cryoprotectant solution (ethylene glycol, glycerol, 0.5M PB, NaCl, KCl, in dH_20) at -20°C. Free floating sections were washed three times with PBS, then pre-incubated with permeabilizing agent 0.3% Triton X in PBS for 30 min. Sections were incubated in blocking buffer (20% donkey serum, 1% BSA, 0.1% glycine, 0.1% lysine in PBS) for 1hr. This was followed by overnight incubation at 4°C with primary antibodies in incubation

buffer (5% donkey serum, 1% BSA, 0.1% glycine, and 0.1% lysine). Primary antibodies used in this study were: mouse anti-serine racemase (BD biosciences, cat #612052), rabbit anti-PSD95 (Abcam, cat #12093), rabbit anti-MAP2 (Abcam, cat# 5622). Sections were washed three times with PBS, then incubated with the appropriate secondary antibodies in incubation buffer for 1hr. The following isotype-specific secondary antibodies were used: donkey anti-mouse Alexa 488, donkey anti-rabbit Alexa 568 with, donkey anti-rabbit Alexa 647, goat anti-mouse Alexa 488, and goat anti-rabbit Alexa 568. After secondary antibody incubation, tissues were washed three times with 1x PBS. Before mounting on Fisherbrand Superfrost Plus glass microscope slides, free-floating slices were rinsed with water and counterstained using the nuclear maker DAPI. Finally, glass slides were covered using cover glass with Vectashield antifade mounting media (Vectorlabs). Confocal images were acquired using a Leica SP8 confocal microscope (20x/40x objectives) and Z-series stack confocal images were taken at fixed intervals using consistent settings.

Electron Microscopy

Two month-old mice were deeply anesthetized, briefly intracardially perfused with cold PBS (0.5M phosphate buffer, NaCl, pH 7.4), followed by either (3% glutaraldehyde, 1% paraformaldehyde and 0.2% sodium metabisulfite in 0.1M phosphate buffer, pH7.4) for D-serine nanogold staining(Balu et al., 2014) or (4% paraformaldehyde and 0.5% glutaraldehyde in 0.1M PB pH7.4) for SR DAB staining. Brains were post-fixed in either $CaCl_2$, 0.1% sucrose, 3% glutaraldehyde, 1% PFA in dH_20 (pH 7.4; D-serine staining) or 4% PFA, 0.1% sucrose, 0.5% glutaraldehyde (pH 7.4; SR

staining). Brains were washed with 0.1 M PB three times for 10 min, and sectioned using a Leica VT1200S Vibratome at 40 μm and stored in cryoprotectant at -20°C.

Nanogold staining: 1.5mm discs were punched out of CA1 region of hippocampal slices, punches were immediately transferred into a 0.1 mm deep cavity of aluminum platelets (type A) filled with 20% BSA as cryoprotectant for high-pressure freezing and covered with a type B platelet (flat side) (Wohlwend, Sennwald, Switzerland). Samples were rapidly frozen using a Leica HPM-100 high-pressure freezer. Frozen samples were transferred in cryo-vials filled with 0.1% uranyl acetate in anhydrous acetone and placed in a precooled Leica EM-AFS2 machine at -95°C. After an hour, the temperature was increased to –90°C, and the samples were kept at this temperature for the next 3 days. The temperature was then increased to -45 °C for 9 hr, followed by three baths of extra-dry acetone for 20 min each at -45 °C, and then embedded flat in Lowicryl HM20 Embedding Media (EMS, cat #14340). Punches were embedded in an increase concentration (10%, 25%, 50%, 75%) of HM20 in anhydrous acetone for 4 hr each at -25 °C, followed by 100% HM20 for 10hrs. at -25 °C, four times. The HM20 embedded punches were polymerized using the UV lamp on the Leica AFS-2 machine at -25 °C for 48 hr, the temperature was increased progressively to 20 °C for the next 9 hr and held at 20 °C for the next 4 days. Punches were sectioned at 70nm using the Reichert-Jung Ultracut E ultramicrotome, sections were placed on nickel slot grids (EMS, cat#G2010-Ni) covered with Formvar support film and immediately followed by immunogold labelling.

Sections were washed with filtered (0.05M TBS pH 7.4 with 0.15% glycine) for 10 min, incubated with filtered (2% normal goat serum in 0.05M TBS, pH 7.4) for 10

min, and then incubated with rabbit anti-D-serine antibody (1:750, Abcam, #6472) with 0.05mM L-serine-BSA-glutaraldehyde conjugate in 2% normal goat serum in 0.05M TBS, pH 7.4, adjusted from (Balu et al., 2014). We previously validated this D-serine IHC protocol using SRKO tissue to demonstrate the necessity of L-serine blocking conjugate inclusion to prevent antibody cross reactivity with L-serine, which is highly expressed in astrocytes (Yang et al., 2010). Following incubation, sections were washed (0.05M TBS pH 7.4) five times for 2 min, incubated in 2% NGS in 0.05M TBS pH8.2 for 5 min, and then incubated with goat anti-rabbit IgG H&L (10nm Gold; 1:20, Abcam cat# 39601) in filtered 2% normal goat serum (0.05 M TBS; pH 8.2) for 2 hr. Sections were washed in 0.05M TBS pH 7.4 six times for 2 min, incubated in 2% glutaraldehyde in 0.05M TBS pH7.4 for 5 min, washed in 0.05M TBS pH 7.4 twice for 2 min, and then in dd$H_2$0 three times for 2 min. Before being imaged, sections were post-stained with filtered uranyl acetate (saturated solution) for 15 min, washed in dd$H_2$0 by dipping 20 times, then incubated in Reynold's lead citrate for 7 min. Sections were imaged using a JEOL JEM-1200 EX II with a 1k CCD.

DAB (3,3′-Diaminobenzidine): Endogenous peroxidases were quenched by incubating sections with 0.3% H_2O_2 in 0.01M PBS for 15 min. Sections were washed in wash buffer 1 (0.01% Triton X-100 in 0.01M PBS) three times and then incubated with 0.05% fresh $NaBH_4$ containing 0.1% glycine for 30min to quench aldehydes. Sections were washed with 0.01M PBS three times, and blocked in (4% BSA, 10% normal goat serum, 0.01% triton-X-100 in 0.01M PBS) for one hour at RT. Sections were washed once with wash buffer 1 and incubated for two days at 4°C with mouse anti-SR antibody (1:1,000; BD Biosciences; cat #612052). Sections were washed with buffer 1, three times for 5 min

and incubated in horse anti-mouse IgM -biotinylated (vector labs BA-2020; 1:500) in blocking buffer for 2 hr at RT. Sections were washed with buffer 1. Sections were incubated for 2 hr at RT with strepavidin–HRP (Invitrogen; Cat #434323; 1:5000) in buffer 1. Sections were washed twice in 0.1M phosphate buffer, incubated sections with DAB - H_2O_2 (Vector; Cat #4105) made in 0.01M Na cacodylate for 5 min, and then washed twice with 0.1M PB. Sections were post fixed in 1% OsO_4 for 30 min, dehydrated in graded ethanol series and extra dry acetone, and flat embedded in Embed 812 resin. Ultrathin sections (~80 nm) were collected on Formvar-coated slot grids (EMS, Cat #G2010-Cu). Some of the sections were imaged without staining and some were post-stained with uranyl acetate (saturated solution) and Reynold's lead citrate, before being imaged. Unstained/stained sections were imaged on a JEOL JEM-1200 EX II with an 1k CCD camera, and on a Tecnai F20 (200 keV) transmission electron microscope (FEI, Hillsboro, OR) and recorded using a 2K × 2K charged-coupled device (CCD) camera, at 1900X magnification (1.12 nm pixel size). For large overviews, we acquired montages of overlapping high-magnification images in an automated fashion using the microscope control software SerialEM (Mastronarde, 2005).

Electrophysiology

Postnatal viral injection: Neonatal [P0-P1] *Srr*$^{fl/fl}$ mice of both sexes were stereotaxically injected with high-titer rAAV1-Cre:GFP viral stock (~1-5 x 10^{12} vg/mL) with coordinates targeting CA1 of hippocampus as previously described (Gray et al., 2011). Transduced neurons were identified by nuclear GFP expression. Cre expression was generally limited to the hippocampus within a sparse population of CA1 pyramidal neurons.

Acute slice preparation: Mice older than P30 were anesthetized with isoflurane and transcardially perfused with ice-cold artificial cerebrospinal fluid (ACSF), containing (in mM) 119 NaCl, 26.2 $NaHCO_3$, 11 glucose, 2.5 KCl, 1 NaH_2PO_4, 2.5 $CaCl_2$ and 1.3 $MgSO_4$. Modified transverse 300 μm slices of dorsal hippocampus were prepared by performing a ~10° angle blocking cut of the dorsal portion of each cerebral hemisphere (Bischofberger et al., 2006) then mounting the cut side down on a Leica VT1200 vibratome in ice-cold ACSF. Slices were incubated in 32°C NMDG solution containing (in mM) 93 NMDG, 93 HCl, 2.5 KCl, 1.2 NaH_2PO_4, 30 $NaHCO_3$, 20 HEPES, 25 glucose, 5 sodium ascorbate, 2 thiourea, 3 sodium pyruvate, 10 $MgSO_4$, and 0.5 $CaCl_2$ (Ting et al., 2018) for 15 min, transferred to room temperature ACSF, and held for at least 1 hr before recording. Mice younger than P30 were anesthetized in isoflurane and decapitated. Brains were rapidly removed and placed in ice-cold sucrose cutting buffer, containing the following (in mM): 210 sucrose, 25 $NaHCO_3$, 2.5 KCl, 1.25 NaH_2PO_4, 7 glucose, 7 $MgCl_2$, and 0.5 $CaCl_2$. Slices were cut in sucrose cutting buffer as described above. Slices were recovered for 1 hr in 32°C ACSF. All solutions were vigorously perfused with 95% O_2 and 5% CO_2. Slices were transferred to a submersion chamber on an upright Olympus microscope, perfused in room temperature ACSF containing picrotoxin (0.1 mM), and saturated with 95% O_2 and 5% CO_2. CA1 neurons were visualized by infrared differential interference contrast microscopy, and GFP+ cells were identified by epifluorescence microscopy.

Whole-cell patch clamp: Cells were patched with 3-5 MΩ borosilicate pipettes filled with intracellular solution containing (in mM) 135 cesium methanesulfonate, 8 NaCl, 10

HEPES, 0.3 Na-GTP, 4 Mg-ATP, 0.3 EGTA, and 5 QX-314. Series resistance was monitored and not compensated, and cells were discarded if series resistance varied more than 25%. All recordings were obtained with a Multiclamp 700B amplifier (Molecular Devices), filtered at 2 kHz, and digitized at 10 Hz. All EPSCs were evoked at 0.1Hz. AMPA receptor EPSCs were recorded at -70mV. NMDAR-EPSCs were recorded in the presence of 10μM NBQX at +40mV with the exception of D-serine wash experiments, which were recorded at -40mV (Bergeron et al., 1998; Basu et al., 2009). Dual-whole cell recordings are the average response of approximately 40 sweeps, the typical recording length. Paired pulse response (PPR) was performed with two sequential EPSCs at a 50 ms interval. LTP was induced by depolarization to 0mV paired with 1Hz stimulation for 90 s. R025-6981 (R025) and D-serine wash experiments recorded NMDAR-EPSCs by coming to a steady 5 min baseline before proceeding with wash. EPSC amplitude was determined by measuring the peak of the response compared to pre-stimulation baseline. All summary amplitude graphs after a time course experiment average the last 5 min of data compared to baseline. EPSC charge transfer was determined by measuring the area of the response compared to pre-stimulation baseline. EPSC decay time was measured as the time between EPSC peak amplitude and 63% decay from the peak. Analysis was performed with the Clampex software suite (Molecular Devices).

Experimental design and statistical analysis

All data represents the mean ± SEM of n = number of neurons or pairs of neurons. In electrophysiology experiments, two to three data points were typically acquired per mouse. Experiments include both males and females. Data were analyzed using

Clampfit 10.4 (Axon Instruments) and Prism 8 software (GraphPad). Data were analyzed using an unpaired *t* test for LTP and exogenous D-serine wash recordings, a ratio-paired *t* test for paired amplitude data, and paired *t* test for decay kinetics. In all cases, $p<0.05$ was considered significant. For TEM, micrographs were visualized on IMOD software (Kremer et al., 1996), and clearly defined synapses (pre- and post-neurons) were identified and all postsynaptic neurons were manually counted for nanogold labeled D-serine. No D-serine was detected in the presynaptic neuron. For SR quantification, in Image J, a region of interest (ROI) was drawn around fifty synapses for both SR labeled and control (no antibody) sections; pixel intensity was quantified per ROI for each synapse.

Results

Postsynaptic localization of serine racemase and D-serine

Biochemical evidence from adult rat brain demonstrated the presence of SR in synaptic compartments (Balan et al., 2009), while in primary mouse neuronal cortical cultures, SR and D-serine co-localize with PSD-95 and NMDARs (GluN1) in postsynaptic glutamatergic synapses, but not in pre-synaptic terminals (Ma et al., 2014; Lin et al., 2016). Furthermore, SR expression is developmentally regulated in the mouse brain, with low levels early postnatally and peaking ~P28 (Miya et al., 2008; Basu et al., 2009). In the CA1 subfield of dorsal hippocampus at P16 (Fig 1A,B), a low and diffuse expression of SR was detected in apical dendrites of *stratum radiatum* (*s.r.*), and no staining was seen in SR-/- mice. By two months of age, there is robust SR expression throughout CA1, including high levels in apical dendrites as demonstrated by co-

localization with microtubule-associated protein 2 (MAP2; Fig 1C). Using immuno-electron microscopy (EM), we show that SR is present in CA1 apical dendrites of *s.r.*, with no SR immunoreactivity in control sections, in which only the primary SR antibody was omitted (Fig 1D,E).

We also examined whether SR was localized to postsynaptic compartments in *s.r.* of CA1. We found a more intense DAB product as determined by the pixel intensity per region of interest (ROI) at postsynaptic densities (PSDs) in SR-antibody stained sections compared to control sections with no primary antibody, demonstrating the presence of SR in dendritic spines (Fig 2A-C; average pixel intensity/area; No 1° Ab, 78.0 ± 11.4 (SD), n = 48; SR Ab, 110.6 ± 15.3 (SD), n = 50). However, we did not detect SR immunoreactivity in presynaptic compartments (Fig 2B). Using dual-antigen immunofluorescence, we also demonstrate co-localization of SR with the PSD marker, PSD-95 in CA1 (Fig 2D).

Since we detected the enzyme SR in dendrites and spines, we next examined whether the NMDAR co-agonist D-serine is also localized to these compartments. Using immuno-EM and a D-serine immunostaining protocol that we previously validated using SRKO mice (Balu et al., 2014), we observed high numbers of nanogold particles in CA1 *stratum radiatum (s.r.)* dendrites, while we did not detect any dendritic nanogold particle binding in control sections that omitted only D-serine primary antibody (Fig 3A-C). Finally, we detected nanogold particles postsynaptically in dendritic spines in CA1, but not in pre-synaptic compartments or in control sections that were not incubated with the D-serine primary antibody (Fig 4A-C).

Single-neuron genetic deletion of serine racemase does not alter synaptic function in P16-21 CA1

To examine the physiological function of postsynaptic SR, we utilized a single-neuron genetic approach in SR conditional knockout mice. Here, SR was removed in a sparse subset of CA1 pyramidal neurons by postnatal day 0 (P0) stereotaxic injection of adeno-associated virus, serotype 1 expressing a Cre recombinase GFP fusion protein (AAV1-Cre:GFP) into floxed SR (*Srr*$^{fl/fl}$) mice (Fig 5A). This mosaic transduction allows for simultaneous whole-cell recordings from Cre-expressing (Cre+) and neighboring untransduced neurons (control) (Fig 5B), providing a rigorous comparison of the cell-autonomous effects of SR deletion while controlling for presynaptic input (Gray et al., 2011).

Glycine is thought to be the primary synaptic NMDAR co-agonist at early developmental stages before being gradually supplanted by D-serine around the third postnatal week in CA1 (Le Bail et al., 2015). Therefore, we first assessed the contribution of postsynaptic SR to synaptic physiology at P16-21. In P16-21 mice, we found no difference in the NMDAR-EPSC amplitudes between control and Cre+ neurons (Fig 5C; control: 131.7 ± 25.9 pA, n = 11; Cre+: 114.0 ± 24.4 pA, n = 11; t(10) = 1.625, p = 0.1351, ratio paired *t* test). Decay kinetics of NMDAR-EPSCs, measured as the time between the EPSC peak and 63% decay, were also unchanged (Fig 5D; control: 170.0 ± 7.5 ms, n = 10; Cre+: 173.1 ± 10.8 ms, n = 10; t(9) = 0.2197, p = 0.8310, paired *t* test). We also recorded AMPAR-EPSCs from P16-21 mice in a pairwise manner and likewise found no change in AMPAR-EPSCs (Fig 5E; control: 85.9 ± 22.3 pA, n = 9; Cre+: 91.0 ± 20.2 pA, n = 9; t(8) = 0.778, p = 0.459, ratio paired *t* test). Finally, we recorded paired pulse ratios (PPR) with a 50 ms interval from control and Cre+ neurons and found no change

in PPR (Fig 5F; 2.21 ± 0.28, n = 4; Cre+: 1.94 ± 0.21, n = 4; t(6) = 0.7694, p = 0.4708, *t* test). As expected, postsynaptic SR deletion has no observed effect on synaptic function in P16-21 CA1 consistent with glycine being the primary synaptic co-agonist at this time-point.

Single-neuron genetic deletion of serine racemase reduces NMDAR-EPSCs in P45-70 CA1

Next, we performed recordings around 2 months of age when D-serine is clearly the primary synaptic NMDAR co-agonist (Papouin et al., 2012; Le Bail et al., 2015). In P45-70 mice, we found that postsynaptic SR deletion decreased NMDAR-EPSCs in Cre+ neurons (Fig 6A; control: 144.1 ± 18.9 pA, n = 19; Cre+: 87.6 ± 11.7 pA, n = 19; t(18) = 3.689, p = 0.0017, ratio paired *t* test). Importantly, AMPAR-EPSCs were unchanged indicating that the effect was specific to NMDARs (Fig 6B; control: 111.8 ± 19.0 pA, n = 14; Cre+: 85.4 ± 15.7 pA, n = 14; t(13) = 1.936, p = 0.0749, ratio paired *t* test). PPR was also unchanged (Fig 6C; control: 1.83 ± 0.15, n = 9; Cre+: 1.70 ± 0.22, n = 9; t(16) = 0.4649, p = 0.6483, *t* test), suggesting that the NMDAR-EPSC decrease was postsynaptic in origin. Previous studies have demonstrated that acute removal of NMDAR co-agonists impairs synaptic plasticity (Papouin et al., 2012; Le Bail et al., 2015) and that germline and neuron-specific SR deletion reduces LTP (Basu et al., 2009; Benneyworth et al., 2012; Balu et al., 2013; Perez et al., 2017). Therefore, we assessed the effect of single cell postsynaptic deletion of SR on LTP. Surprisingly, we found that LTP was unchanged in Cre+ neurons (Fig 6D; control: 193.9 ± 22.1 %, n = 12; Cre+: 196.6 ± 15.1 %, n = 12; t(22) = 0.09961, p = 0.9216, *t* test).

Single-neuron genetic deletion of serine racemase upregulates GluN2B in P45-70 CA1

We next sought to understand the discrepancy between the reduced NMDAR-EPSC amplitude and, in contrast to previous studies, the lack of effect on LTP (Basu et al., 2009; Benneyworth et al., 2012; Balu et al., 2013; Perez et al., 2017). We hypothesized that the reduced NMDAR-EPSC amplitude might be due to a decreased synaptic co-agonist concentration and thus less occupancy of the NMDAR co-agonist sites. To test this, we washed a saturating concentration of exogenous D-serine onto slices while recording from control and Cre+ neurons. If synaptic NMDARs had reduced co-agonist saturation in Cre+ relative to control cells, exogenous D-serine would be predicted to cause a greater enhancement of the NMDAR-EPSC amplitude in the Cre+ cells. However, we found that there was no significant difference in the potentiation of Cre+ and control cells in response to 100 μM D-serine (Fig 7A; control: 125.6 ± 4.1 %, n = 14; Cre+: 117.4 ± 14.4 %, n = 7; $t(19) = 0.7147$, $p = 0.4835$, *t* test).

Interestingly, the decay kinetics of NMDAR-EPSCs were found to be significantly longer in Cre+ neurons (Fig 7B; control: 191.1 ± 12.1 ms, n = 19; Cre+: 288.6 ± 30.6 ms, n = 19; $t(18) = 3.040$, $p = 0.0070$, paired *t* test). Since prolonged decay of synaptic NMDAR-EPSCs likely indicates an increased proportion of the GluN2B subunit, we tested this pharmacologically with the GluN2B-selective inhibitor Ro25-6981 (Ro25) (Fischer et al., 1997). We found Cre+ neurons were significantly more sensitive than control neurons to 5 μM Ro25 (Fig 7C; control: 24.8 ± 8.7 %, n = 6; Cre+: 61.2 ± 14.5 %, n = 4; $t(8) = 2.340$, $p = 0.0474$, *t* test), demonstrating an increase in the synaptic GluN2B/GluN2A ratio.

GluN2B-containing NMDARs have lower peak open probability compared to GluN2A-containing NMDARs (Chen et al., 1999; Erreger et al., 2005; Gray et al., 2011). Though because their single channel conductances are identical (Stern et al., 1992), a reduction in the macroscopic EPSC amplitude could represent similar numbers of synaptic NMDARs. Indeed, the combination of reduced peak amplitude with the prolonged decay kinetics resulted in no significant change in charge transfer of Cre+ neurons (Fig 7D; control: 40.2 ± 5.4 pC, n = 19; Cre+: 32.3 ± 3.9 pC, n = 19; t(18) = 1.518, p = 0.1464, paired *t* test) consistent with a similar overall number of synaptic NMDARs. Overall, this increase in the GluN2B/GluN2A ratio may represent a homeostatic mechanism to maintain synaptic plasticity.

Single-neuron genetic deletion of serine racemase impairs LTP in P23-39 CA1

Since the normal LTP in P45-70 mice might be due to homeostatic increases in GluN2B in the chronic absence of SR, we next examined an intermediate time-point when D-serine is expected to be the primary synaptic co-agonist (Le Bail et al., 2015) but compensatory changes may not have yet occurred. Examining mice from the 4^{th}-5^{th} week of life (P23-39), we found that the NMDAR-EPSCs and their decay kinetics were unchanged in Cre+ neurons (NMDAR-EPSCs, Fig 8A; control: 91.7 ± 27.7 pA, n = 9; Cre+: 140.8 ± 26.3 pA, n = 9; t(8) = 1.879, p = 0.0970, ratio paired *t* test; decay, Fig 8B; control: 200.8 ± 19.4 ms, n = 7; Cre+: 268.3 ± 60.4 ms, n = 7; t(6) = 1.510, p = 0.1818, paired *t* test). Similar to other time-points, AMPAR-EPSCs (Fig 8C; 60.8 ± 12.7 pA, n =11; Cre+: 73.4 ± 10.4 pA, n = 11; t(10) = 1.724, p = 0.1155, ratio paired *t* test) and PPR (Fig 8D; control: 2.06 ± 0.21, n = 5; Cre+: 2.05 ± 0.12; t(8) = 0.01663, p = 0.9871, *t* test)

were unchanged. Interestingly, LTP was completely eliminated in Cre+ neurons at P23-39 and restored by exogenous D-serine applied until the end of the induction period (Fig 8E; control: 151.9 ± 10.3 %, n = 8; Cre+: 100.2 ± 6.1 %, n = 6; Cre+ with D-serine: 164.8 ± 15.3 %, n = 8; control to Cre+: $t(12) = 3.955$, $p = 0.0019$, *t* test; control to Cre+ with D-serine: $t(14) = 0.7032$, $p = 0.4934$, *t* test), demonstrating that neuronal SR cell-autonomously regulates NMDAR function and synaptic plasticity in CA1 pyramidal cells.

Discussion

Despite the recognized importance of D-serine in NMDAR function and synaptic plasticity, our understanding of the regulation of D-serine synthesis, release, and degradation remains quite limited. Indeed, even the cellular source of D-serine has been contested (Wolosker et al., 2016; Papouin et al., 2017; Wolosker et al., 2017). Early studies suggested that D-serine is exclusively synthesized and released by astrocytes (Schell et al., 1995; Schell et al., 1997; Wolosker et al., 1999) leading to the classification of D-serine as a gliotransmitter (Wolosker et al., 2002; Miller, 2004; Panatier et al., 2006). More recent studies, using the SR knockout mice as controls, have strongly supported a predominantly neuronal localization [recently reviewed by (Wolosker et al., 2016)]. In this study, we demonstrate for the first time a cell-autonomous role for neuronal SR in regulating synaptic NMDAR function. Specifically, we find that single-neuron deletion of SR impairs LTP, although LTP is restored later with a concomitant upregulation of GluN2B. Furthermore, in agreement with previous studies in cultured neurons (Ma et al., 2014; Lin et al., 2016), we found that SR localizes to the apical dendrites and the postsynaptic density *in situ* in hippocampal CA1 pyramidal neurons.

We have also identified D-serine in dendrites and postsynaptic compartments by immunogold EM. Together, these results provide strong evidence for the neuronal localization and cell-autonomous function of SR in the intact hippocampus. In addition, these findings together suggest a possible autocrine mode of D-serine action at synapses.

Regulation of LTP by postsynaptic serine racemase

We demonstrate that single-neuron SR deletion cell-autonomously impairs LTP in P23-39 mice. Deficits in neuronal D-serine have been repeatedly shown to reduce LTP. Germline SR knockout mice show reduced LTP in CA1 (Basu et al., 2009; Balu et al., 2016; Neame et al., 2019), dentate gyrus (Balu et al., 2013), and lateral amygdala (Li et al., 2013). Furthermore, neuron-specific SR knockout mice show reduced LTP while astrocyte-specific SR knockout mice have normal LTP (Benneyworth et al., 2012; Perez et al., 2017). Similarly, acute enzymatic depletion of D-serine reduces the magnitude of LTP in CA1 (Yang et al., 2003; Papouin et al., 2012; Rosenberg et al., 2013; Le Bail et al., 2015), visual cortex (Meunier et al., 2016), nucleus accumbens (Curcio et al., 2013), and lateral amygdala (Li et al., 2013). Together, these studies suggest that neuronally-derived D-serine is crucial for synaptic plasticity. Additionally, the cell-autonomous loss of LTP, and rescue by exogenous D-serine, seen here suggests a possible autocrine mode of D-serine action (discussed below). Surprisingly, this loss of LTP occurred without a reduction in the amplitude of the NMDAR-EPSCs, arguing that baseline co-agonist occupancy is not significantly altered, perhaps through compensation by glycine, or through D-serine diffusing from neighboring neurons. However, during plasticity, higher concentrations of co-agonist may be required. Indeed, co-agonist occupancy of synaptic NMDARs can be altered by activity (Panatier et al., 2006; Li et al., 2009), and

446 glutamate binding reduces the affinity of the NMDAR glycine-site up to seven-fold
447 (Mayer et al., 1989; Lester et al., 1993; Cummings and Popescu, 2015), suggesting
448 additional co-agonist release might be needed during plasticity, especially during high
449 frequency induction protocols not tested in this study.

450 Interestingly, we found LTP was restored by P45, possibly through a homeostatic
451 process. This restoration of LTP was associated with an upregulation of synaptic
452 GluN2B. Indeed, a prolongation of the NMDAR-EPSC decay kinetics has been
453 previously reported in the germline SR knockout mice (Basu et al., 2009), and GluN2B
454 is known to promote LTP through its unique array of c-tail interacting proteins (Foster
455 et al., 2010). Importantly, the enhancement of GluN2B subunits in CA1 could directly
456 compensate for a lack of D-serine. GluN2A and GluN2B allosterically regulate co-agonist
457 potency at the GluN1 glycine binding site (Priestley et al., 1995; Madry et al., 2007; Chen
458 et al., 2008; Maolanon et al., 2017) with a two- to five-fold higher potency of co-agonists
459 at GluN2B-containing NMDARs. Therefore, enhancement of GluN2B could compensate
460 for a loss of D-serine given a smaller but stable pool of synaptic glycine. Indeed, this
461 increase in GluN2B could explain the lack of NMDAR saturation changes in the P45-P70
462 mice. Other groups using the SR germline KO or the broad neuronal SR deletion,
463 however, did not observe this restoration of LTP (Basu et al., 2009; Balu et al., 2016;
464 Perez et al., 2017; Neame et al., 2019). Perhaps in the single-neuron SR deletion there is
465 some degree of D-serine spillover from neighboring neurons that is sufficient to fully
466 activate the higher-affinity GluN2B-containing NMDARs and restore LTP, whereas
467 when SR is deleted from all neurons, this spillover is eliminated.

468 The increase in synaptic GluN2B, however, might solely be an associated finding.
469 One possibility is that NMDAR synaptic stability is regulated by co-agonist composition

in a subunit-specific manner. Indeed, co-agonist binding primes NMDARs for internalization and recycling (Nong et al., 2003), and D-serine administration onto dissociated cortical cultures increases the rate of GluN2B surface diffusion and decreases residence at postsynaptic sites (Papouin et al., 2012; Ferreira et al., 2017), which may be required for LTP (Dupuis et al., 2014). Thus, loss of D-serine at synaptic sites by the removal of SR may alter the balance of synaptic GluN2 subunits through changes in trafficking mechanisms and have complex effects on synaptic plasticity.

Autocrine mode of D-serine action?

The postsynaptic localization of SR and the cell-autonomous regulation of NMDAR function by neuronal SR suggests the local postsynaptic release and autocrine mode of D-serine action at synapses. For example, in addition to pyramidal neurons, SR and D-serine also localize to GABAergic neurons (Miya et al., 2008; Curcio et al., 2013; Balu et al., 2014; Lin et al., 2016; Takagi et al., 2020), arguing against D-serine being released presynaptically as a co-transmitter. Furthermore, recent work suggests that postsynaptic SR activity is tightly regulated by AMPAR and NMDAR activity (Balan et al., 2009; Ma et al., 2014; Lin et al., 2016). An autocrine mode of D-serine action is also supported by the identification of D-serine transporters in neurons. Alanine-serine-cysteine transporter 1 (Asc-1) is a neutral amino acid transporter located in neurons (Helboe et al., 2003; Matsuo et al., 2004) that can mediate the bidirectional transport of D-serine while exchanging with other small neutral amino acids (Fukasawa et al., 2000). Stimulating the antiporter activity of Asc-1 by the addition of D-isoleucine induces release of neuronal D-serine from cultured neurons, and enhances LTP in acute hippocampal slices (Rosenberg et al., 2013; Sason et al., 2017). Additionally, inhibition

494 of Asc-1 decreases both D-serine uptake and release and inhibits LTP in CA1 (Sason et
495 al., 2017). However, Asc-1 also transports other amino acids, including glycine and L-
496 serine, which complicates interpretation of its effects (Fukasawa et al., 2000).
497 Furthermore, the subcellular localization of Asc-1 is not known. Recently, the system A-
498 type glutamine transporter SNAT1 has been proposed as a candidate neuronal reuptake
499 transporter for D-serine (Bodner et al., 2020), though the precise localization of SNAT1
500 is also not known.
501
502 ***High levels of non-synaptic serine racemase***
503 As we show here (Fig 1), SR immunoreactivity is curiously high in non-synaptic
504 locations, notably the soma and dendrites, but for what purpose? The broad distribution
505 of SR at P16 might indicate imprecise regulation of D-serine release prior to the
506 compartmentalization of glycine at extrasynaptic NMDARs and D-serine to synaptic
507 NMDARs (Gray and Nicoll, 2012; Papouin et al., 2012), and might explain the lack of
508 effects of single-cell SR deletion at P16 (Fig 5). However, evidence suggests that both
509 nuclear and dendritic localization of SR downregulates its activity. For example,
510 following apoptotic insult, SR translocates to the nucleus independent of NMDAR
511 activity where its racemase activity is inhibited to limit apoptotic damage (Kolodney et
512 al., 2015). Interestingly, in addition to its function as a racemase, SR can also function as
513 an eliminase, catalyzing the α,β-elimination of water from both L-serine (Strisovsky et
514 al., 2003) and D-serine (Foltyn et al., 2005) to form pyruvate. At least *in vitro*, SR
515 produces 3-fold more pyruvate than D-serine, suggesting that the eliminase activity is
516 dominant (Panizzutti et al., 2001; Foltyn et al., 2005). Indeed, these dueling activities of
517 SR may function to limit intracellular D-serine levels (Foltyn et al., 2005). Because its

racemase activity can be controlled by post-translational modifications and protein-protein interactions (Balan et al., 2009; Foltyn et al., 2010; Ma et al., 2014), and racemase and eliminase activity are differentially controlled by coenzyme availability (Strisovsky et al., 2003), SR may have pleotropic roles dependent on subcellular localization. Nevertheless, this study does not ultimately distinguish between SR racemization and elimination.

In summary, our data show the postsynaptic localization of SR in hippocampal CA1 pyramidal neurons and the cell-autonomous regulation of NMDARs by neuronal SR. These results support an autocrine mode of D-serine following postsynaptic release. Indeed, the concept of postsynaptic release of neuromodulators is not new. For example, brain-derived neurotrophic factor (BDNF) is released postsynaptically during synaptic plasticity (Harward et al., 2016; Hedrick et al., 2016). However, further studies are needed to identify the mechanisms regulating D-serine postsynaptic release and termination of D-serine action within the synaptic cleft.

References

Balan L, Foltyn VN, Zehl M, Dumin E, Dikopoltsev E, Knoh D, Ohno Y, Kihara A, Jensen ON, Radzishevsky IS, Wolosker H (2009) Feedback inactivation of D-serine synthesis by NMDA receptor-elicited translocation of serine racemase to the membrane. Proc Natl Acad Sci U S A 106:7589-7594.

Balu DT, Takagi S, Puhl MD, Benneyworth MA, Coyle JT (2014) D-serine and serine racemase are localized to neurons in the adult mouse and human forebrain. Cell Mol Neurobiol 34:419-435.

Balu DT, Li Y, Puhl MD, Benneyworth MA, Basu AC, Takagi S, Bolshakov VY, Coyle JT (2013) Multiple risk pathways for schizophrenia converge in serine racemase knockout mice, a mouse model of NMDA receptor hypofunction. Proc Natl Acad Sci U S A 110:E2400-2409.

Balu DT, Presti KT, Huang CCY, Muszynski K, Radzishevsky I, Wolosker H, Guffanti G, Ressler KJ, Coyle JT (2018) Serine Racemase and D-serine in the Amygdala Are Dynamically Involved in Fear Learning. Biol Psychiatry 83:273-283.

Balu DT, Li Y, Takagi S, Presti KT, Ramikie TS, Rook JM, Jones CK, Lindsley CW, Conn PJ, Bolshakov VY, Coyle JT (2016) An mGlu5-Positive Allosteric Modulator Rescues the Neuroplasticity Deficits in a Genetic Model of NMDA Receptor Hypofunction in Schizophrenia. Neuropsychopharmacology 41:2052-2061.

Basu AC, Tsai GE, Ma CL, Ehmsen JT, Mustafa AK, Han L, Jiang ZI, Benneyworth MA, Froimowitz MP, Lange N, Snyder SH, Bergeron R, Coyle JT (2009) Targeted disruption of serine racemase affects glutamatergic neurotransmission and behavior. Mol Psychiatry 14:719-727.

Benneyworth MA, Li Y, Basu AC, Bolshakov VY, Coyle JT (2012) Cell selective conditional null mutations of serine racemase demonstrate a predominate localization in cortical glutamatergic neurons. Cell Mol Neurobiol 32:613-624.

556 Bergeron R, Meyer TM, Coyle JT, Greene RW (1998) Modulation of N-methyl-D-aspartate receptor
557 function by glycine transport. Proc Natl Acad Sci U S A 95:15730-15734.
558 Bischofberger J, Engel D, Li L, Geiger JR, Jonas P (2006) Patch-clamp recording from mossy fiber
559 terminals in hippocampal slices. Nat Protoc 1:2075-2081.
560 Bodner O, Radzishevsky I, Foltyn VN, Touitou A, Valenta AC, Rangel IF, Panizzutti R, Kennedy RT, Billard
561 JM, Wolosker H (2020) D-Serine Signaling and NMDAR-Mediated Synaptic Plasticity Are
562 Regulated by System A-Type of Glutamine/D-Serine Dual Transporters. J Neurosci 40:6489-6502.
563 Chen N, Luo T, Raymond LA (1999) Subtype-dependence of NMDA receptor channel open probability. J
564 Neurosci 19:6844-6854.
565 Chen PE, Geballe MT, Katz E, Erreger K, Livesey MR, O'Toole KK, Le P, Lee CJ, Snyder JP, Traynelis SF,
566 Wyllie DJ (2008) Modulation of glycine potency in rat recombinant NMDA receptors containing
567 chimeric NR2A/2D subunits expressed in Xenopus laevis oocytes. J Physiol 586:227-245.
568 Cummings KA, Popescu GK (2015) Glycine-dependent activation of NMDA receptors. J Gen Physiol
569 145:513-527.
570 Curcio L, Podda MV, Leone L, Piacentini R, Mastrodonato A, Cappelletti P, Sacchi S, Pollegioni L, Grassi C,
571 D'Ascenzo M (2013) Reduced D-serine levels in the nucleus accumbens of cocaine-treated rats
572 hinder the induction of NMDA receptor-dependent synaptic plasticity. Brain 136:1216-1230.
573 Ding X, Ma N, Nagahama M, Yamada K, Semba R (2011) Localization of D-serine and serine racemase in
574 neurons and neuroglias in mouse brain. Neurol Sci 32:263-267.
575 Dupuis JP, Ladepeche L, Seth H, Bard L, Varela J, Mikasova L, Bouchet D, Rogemond V, Honnorat J, Hanse
576 E, Groc L (2014) Surface dynamics of GluN2B-NMDA receptors controls plasticity of maturing
577 glutamate synapses. EMBO J 33:842-861.
578 Ehmsen JT, Ma TM, Sason H, Rosenberg D, Ogo T, Furuya S, Snyder SH, Wolosker H (2013) D-serine in
579 glia and neurons derives from 3-phosphoglycerate dehydrogenase. J Neurosci 33:12464-12469.

Erreger K, Dravid SM, Banke TG, Wyllie DJ, Traynelis SF (2005) Subunit-specific gating controls rat NR1/NR2A and NR1/NR2B NMDA channel kinetics and synaptic signalling profiles. J Physiol 563:345-358.

Ferreira JS, Papouin T, Ladepeche L, Yao A, Langlais VC, Bouchet D, Dulong J, Mothet JP, Sacchi S, Pollegioni L, Paoletti P, Oliet SHR, Groc L (2017) Co-agonists differentially tune GluN2B-NMDA receptor trafficking at hippocampal synapses. Elife 6.

Fischer G, Mutel V, Trube G, Malherbe P, Kew JN, Mohacsi E, Heitz MP, Kemp JA (1997) Ro 25-6981, a highly potent and selective blocker of N-methyl-D-aspartate receptors containing the NR2B subunit. Characterization in vitro. J Pharmacol Exp Ther 283:1285-1292.

Foltyn VN, Zehl M, Dikopoltsev E, Jensen ON, Wolosker H (2010) Phosphorylation of mouse serine racemase regulates D-serine synthesis. FEBS Lett 584:2937-2941.

Foltyn VN, Bendikov I, De Miranda J, Panizzutti R, Dumin E, Shleper M, Li P, Toney MD, Kartvelishvily E, Wolosker H (2005) Serine racemase modulates intracellular D-serine levels through an alpha,beta-elimination activity. J Biol Chem 280:1754-1763.

Foster KA, McLaughlin N, Edbauer D, Phillips M, Bolton A, Constantine-Paton M, Sheng M (2010) Distinct roles of NR2A and NR2B cytoplasmic tails in long-term potentiation. J Neurosci 30:2676-2685.

Fukasawa Y, Segawa H, Kim JY, Chairoungdua A, Kim DK, Matsuo H, Cha SH, Endou H, Kanai Y (2000) Identification and characterization of a Na(+)-independent neutral amino acid transporter that associates with the 4F2 heavy chain and exhibits substrate selectivity for small neutral D- and L-amino acids. J Biol Chem 275:9690-9698.

Gray JA, Nicoll RA (2012) Thinking outside the synapse: glycine at extrasynaptic NMDA receptors. Cell 150:455-456.

602 Gray JA, Shi Y, Usui H, During MJ, Sakimura K, Nicoll RA (2011) Distinct modes of AMPA receptor
603 suppression at developing synapses by GluN2A and GluN2B: single-cell NMDA receptor subunit
604 deletion in vivo. Neuron 71:1085-1101.
605 Harward SC, Hedrick NG, Hall CE, Parra-Bueno P, Milner TA, Pan E, Laviv T, Hempstead BL, Yasuda R,
606 McNamara JO (2016) Autocrine BDNF-TrkB signalling within a single dendritic spine. Nature
607 538:99-103.
608 Hedrick NG, Harward SC, Hall CE, Murakoshi H, McNamara JO, Yasuda R (2016) Rho GTPase
609 complementation underlies BDNF-dependent homo- and heterosynaptic plasticity. Nature
610 538:104-108.
611 Helboe L, Egebjerg J, Moller M, Thomsen C (2003) Distribution and pharmacology of alanine-serine-
612 cysteine transporter 1 (asc-1) in rodent brain. Eur J Neurosci 18:2227-2238.
613 Ishiwata S, Umino A, Balu DT, Coyle JT, Nishikawa T (2015) Neuronal serine racemase regulates
614 extracellular D-serine levels in the adult mouse hippocampus. J Neural Transm (Vienna)
615 122:1099-1103.
616 Johnson JW, Ascher P (1987) Glycine potentiates the NMDA response in cultured mouse brain neurons.
617 Nature 325:529-531.
618 Kartvelishvily E, Shleper M, Balan L, Dumin E, Wolosker H (2006) Neuron-derived D-serine release
619 provides a novel means to activate N-methyl-D-aspartate receptors. J Biol Chem 281:14151-
620 14162.
621 Kleckner NW, Dingledine R (1988) Requirement for glycine in activation of NMDA-receptors expressed in
622 Xenopus oocytes. Science 241:835-837.
623 Kolodney G, Dumin E, Safory H, Rosenberg D, Mori H, Radzishevsky I, Wolosker H (2015) Nuclear
624 Compartmentalization of Serine Racemase Regulates D-Serine Production: IMPLICATIONS FOR
625 N-METHYL-D-ASPARTATE (NMDA) RECEPTOR ACTIVATION. J Biol Chem 290:31037-31050.

626 Kremer JR, Mastronarde DN, McIntosh JR (1996) Computer visualization of three-dimensional image
627 data using IMOD. J Struct Biol 116:71-76.
628 Le Bail M, Martineau M, Sacchi S, Yatsenko N, Radzishevsky I, Conrod S, Ait Ouares K, Wolosker H,
629 Pollegioni L, Billard JM, Mothet JP (2015) Identity of the NMDA receptor coagonist is synapse
630 specific and developmentally regulated in the hippocampus. Proc Natl Acad Sci U S A 112:E204-
631 213.
632 Lester RA, Tong G, Jahr CE (1993) Interactions between the glycine and glutamate binding sites of the
633 NMDA receptor. J Neurosci 13:1088-1096.
634 Li Y, Krupa B, Kang JS, Bolshakov VY, Liu G (2009) Glycine site of NMDA receptor serves as a
635 spatiotemporal detector of synaptic activity patterns. J Neurophysiol 102:578-589.
636 Li Y, Sacchi S, Pollegioni L, Basu AC, Coyle JT, Bolshakov VY (2013) Identity of endogenous NMDAR
637 glycine site agonist in amygdala is determined by synaptic activity level. Nat Commun 4:1760.
638 Lin H, Jacobi AA, Anderson SA, Lynch DR (2016) D-Serine and Serine Racemase Are Associated with PSD-
639 95 and Glutamatergic Synapse Stability. Front Cell Neurosci 10:34.
640 Ma TM, Paul BD, Fu C, Hu S, Zhu H, Blackshaw S, Wolosker H, Snyder SH (2014) Serine racemase
641 regulated by binding to stargazin and PSD-95: potential N-methyl-D-aspartate-alpha-amino-3-
642 hydroxy-5-methyl-4-isoxazolepropionic acid (NMDA-AMPA) glutamate neurotransmission cross-
643 talk. J Biol Chem 289:29631-29641.
644 Madry C, Mesic I, Betz H, Laube B (2007) The N-terminal domains of both NR1 and NR2 subunits
645 determine allosteric Zn2+ inhibition and glycine affinity of N-methyl-D-aspartate receptors. Mol
646 Pharmacol 72:1535-1544.
647 Maolanon AR, Risgaard R, Wang SY, Snoep Y, Papangelis A, Yi F, Holley D, Barslund AF, Svenstrup N,
648 Hansen KB, Clausen RP (2017) Subtype-Specific Agonists for NMDA Receptor Glycine Binding
649 Sites. ACS Chem Neurosci 8:1681-1687.

650 Mastronarde DN (2005) Automated electron microscope tomography using robust prediction of
651 specimen movements. J Struct Biol 152:36-51.
652 Matsuo H, Kanai Y, Tokunaga M, Nakata T, Chairoungdua A, Ishimine H, Tsukada S, Ooigawa H,
653 Nawashiro H, Kobayashi Y, Fukuda J, Endou H (2004) High affinity D- and L-serine transporter
654 Asc-1: cloning and dendritic localization in the rat cerebral and cerebellar cortices. Neurosci Lett
655 358:123-126.
656 Mayer ML, Vyklicky L, Jr., Clements J (1989) Regulation of NMDA receptor desensitization in mouse
657 hippocampal neurons by glycine. Nature 338:425-427.
658 Meunier CN, Dallerac G, Le Roux N, Sacchi S, Levasseur G, Amar M, Pollegioni L, Mothet JP, Fossier P
659 (2016) D-Serine and Glycine Differentially Control Neurotransmission during Visual Cortex
660 Critical Period. PLoS One 11:e0151233.
661 Miller RF (2004) D-Serine as a glial modulator of nerve cells. Glia 47:275-283.
662 Miya K, Inoue R, Takata Y, Abe M, Natsume R, Sakimura K, Hongou K, Miyawaki T, Mori H (2008) Serine
663 racemase is predominantly localized in neurons in mouse brain. J Comp Neurol 510:641-654.
664 Mothet JP, Parent AT, Wolosker H, Brady RO, Jr., Linden DJ, Ferris CD, Rogawski MA, Snyder SH (2000) D-
665 serine is an endogenous ligand for the glycine site of the N-methyl-D-aspartate receptor. Proc
666 Natl Acad Sci U S A 97:4926-4931.
667 Neame S, Safory H, Radzishevsky I, Touitou A, Marchesani F, Marchetti M, Kellner S, Berlin S, Foltyn VN,
668 Engelender S, Billard JM, Wolosker H (2019) The NMDA receptor activation by d-serine and
669 glycine is controlled by an astrocytic Phgdh-dependent serine shuttle. Proc Natl Acad Sci U S A
670 116:20736-20742.
671 Nong Y, Huang YQ, Ju W, Kalia LV, Ahmadian G, Wang YT, Salter MW (2003) Glycine binding primes
672 NMDA receptor internalization. Nature 422:302-307.

673 Panatier A, Theodosis DT, Mothet JP, Touquet B, Pollegioni L, Poulain DA, Oliet SH (2006) Glia-derived D-
674 serine controls NMDA receptor activity and synaptic memory. Cell 125:775-784.
675 Panizzutti R, De Miranda J, Ribeiro CS, Engelender S, Wolosker H (2001) A new strategy to decrease N-
676 methyl-D-aspartate (NMDA) receptor coactivation: inhibition of D-serine synthesis by converting
677 serine racemase into an eliminase. Proc Natl Acad Sci U S A 98:5294-5299.
678 Papouin T, Henneberger C, Rusakov DA, Oliet SHR (2017) Astroglial versus Neuronal D-Serine: Fact
679 Checking. Trends Neurosci 40:517-520.
680 Papouin T, Ladepeche L, Ruel J, Sacchi S, Labasque M, Hanini M, Groc L, Pollegioni L, Mothet JP, Oliet SH
681 (2012) Synaptic and extrasynaptic NMDA receptors are gated by different endogenous
682 coagonists. Cell 150:633-646.
683 Perez EJ, Tapanes SA, Loris ZB, Balu DT, Sick TJ, Coyle JT, Liebl DJ (2017) Enhanced astrocytic d-serine
684 underlies synaptic damage after traumatic brain injury. J Clin Invest 127:3114-3125.
685 Priestley T, Laughton P, Myers J, Le Bourdelles B, Kerby J, Whiting PJ (1995) Pharmacological properties
686 of recombinant human N-methyl-D-aspartate receptors comprising NR1a/NR2A and NR1a/NR2B
687 subunit assemblies expressed in permanently transfected mouse fibroblast cells. Mol Pharmacol
688 48:841-848.
689 Rosenberg D, Artoul S, Segal AC, Kolodney G, Radzishevsky I, Dikopoltsev E, Foltyn VN, Inoue R, Mori H,
690 Billard JM, Wolosker H (2013) Neuronal D-serine and glycine release via the Asc-1 transporter
691 regulates NMDA receptor-dependent synaptic activity. J Neurosci 33:3533-3544.
692 Sason H, Billard JM, Smith GP, Safory H, Neame S, Kaplan E, Rosenberg D, Zubedat S, Foltyn VN,
693 Christoffersen CT, Bundgaard C, Thomsen C, Avital A, Christensen KV, Wolosker H (2017) Asc-1
694 Transporter Regulation of Synaptic Activity via the Tonic Release of d-Serine in the Forebrain.
695 Cereb Cortex 27:1573-1587.

696 Schell MJ, Molliver ME, Snyder SH (1995) D-serine, an endogenous synaptic modulator: localization to
697 astrocytes and glutamate-stimulated release. Proc Natl Acad Sci U S A 92:3948-3952.
698 Schell MJ, Brady RO, Jr., Molliver ME, Snyder SH (1997) D-serine as a neuromodulator: regional and
699 developmental localizations in rat brain glia resemble NMDA receptors. J Neurosci 17:1604-
700 1615.
701 Stern P, Behe P, Schoepfer R, Colquhoun D (1992) Single-channel conductances of NMDA receptors
702 expressed from cloned cDNAs: comparison with native receptors. Proc Biol Sci 250:271-277.
703 Strisovsky K, Jiraskova J, Barinka C, Majer P, Rojas C, Slusher BS, Konvalinka J (2003) Mouse brain serine
704 racemase catalyzes specific elimination of L-serine to pyruvate. FEBS Lett 535:44-48.
705 Takagi S, Puhl MD, Anderson T, Balu DT, Coyle JT (2020) Serine Racemase Expression by Striatal Neurons.
706 Cell Mol Neurobiol.
707 Ting JT, Lee BR, Chong P, Soler-Llavina G, Cobbs C, Koch C, Zeng H, Lein E (2018) Preparation of Acute
708 Brain Slices Using an Optimized N-Methyl-D-glucamine Protective Recovery Method. J Vis Exp.
709 Wolosker H, Blackshaw S, Snyder SH (1999) Serine racemase: a glial enzyme synthesizing D-serine to
710 regulate glutamate-N-methyl-D-aspartate neurotransmission. Proc Natl Acad Sci U S A 96:13409-
711 13414.
712 Wolosker H, Panizzutti R, De Miranda J (2002) Neurobiology through the looking-glass: D-serine as a new
713 glial-derived transmitter. Neurochem Int 41:327-332.
714 Wolosker H, Balu DT, Coyle JT (2016) The Rise and Fall of the d-Serine-Mediated Gliotransmission
715 Hypothesis. Trends Neurosci 39:712-721.
716 Wolosker H, Balu DT, Coyle JT (2017) Astroglial Versus Neuronal D-Serine: Check Your Controls! Trends
717 Neurosci 40:520-522.
718 Yang JH, Wada A, Yoshida K, Miyoshi Y, Sayano T, Esaki K, Kinoshita MO, Tomonaga S, Azuma N,
719 Watanabe M, Hamase K, Zaitsu K, Machida T, Messing A, Itohara S, Hirabayashi Y, Furuya S

(2010) Brain-specific Phgdh deletion reveals a pivotal role for L-serine biosynthesis in controlling the level of D-serine, an N-methyl-D-aspartate receptor co-agonist, in adult brain. J Biol Chem 285:41380-41390.

Yang Y, Ge W, Chen Y, Zhang Z, Shen W, Wu C, Poo M, Duan S (2003) Contribution of astrocytes to hippocampal long-term potentiation through release of D-serine. Proc Natl Acad Sci U S A 100:15194-15199.

Yoshikawa M, Takayasu N, Hashimoto A, Sato Y, Tamaki R, Tsukamoto H, Kobayashi H, Noda S (2007) The serine racemase mRNA is predominantly expressed in rat brain neurons. Arch Histol Cytol 70:127-134.

Figure Legends

Figure 1: SR is present in the apical dendrites of pyramidal neurons in CA1. **(A-C)** Representative confocal images showing co-localization of SR immunofluorescence (magenta) with microtubule associated protein 2 (MAP2; green) in the apical dendrites of CA1 pyramidal neurons in *stratum radiatum* (*s.r)* at either P16 (**A**; SRKO, **B**; WT) or 2 months (**C**; WT). Scale bars 10μM. **(E-F)** TEM micrographs showing SR DAB photoreaction product in CA1 apical dendrites at 2 months (n = 3 mice). Scale bars = 500 nM

Figure 2: SR is enriched in the PSD of dendritic spines in CA1. **(A,B)** TEM micrographs showing SR DAB photoreaction product in hippocampal synapses of CA1 *stratum radiatum* (*s.r.*). Scale bars = 500 nM. **(C)** Intensity of DAB product at individual postsynaptic densities (PSD) as pixel intensity per region of interest (ROI), sorted to show range. Dashed lines represent average pixel intensity ± SD in shaded bars (No 1° Ab, 78.0 ± 11.4, n = 48; SR Ab, 110.6 ± 15.3, n = 50; n = 1 mouse). **(D)** Representative confocal images of SR immunofluorescence (magneta) showing colocalization with PSD95 (green) at 2 months. Scale bars 10μM; n = 3 mice; *stratum pyramidale* (*pyr*); *stratum radiatum* (*s.r.*).

Figure 3: D-serine is present in apical dendrites of pyramidal neurons in CA1. **(A,B)** TEM micrographs showing D-serine nanogold particles in hippocampal CA1 apical dendrites at 2 months of age. **(C)** Histogram showing the number of D-serine

753 nanogold particles in dendritic segments (n = 1 mouse; 150-500 dendrites). Scale bar –
754 200 nM
755
756 **Figure 4**: D-serine is present in dendritic spines in CA1.
757 **(A,B)** TEM micrographs showing D-serine nanogold particles in dendritic spines in CA1
758 *stratum radiatum* at 2 months of age. **(C)** Histogram showing the number of D-serine
759 nanogold particles in dendritic spines (n = 1 mouse; 130-300 dendritic spines). Scale bar
760 – 100 nM
761
762 **Figure 5**: No effects at P14-21 following single-neuron SR deletion
763 **(A)** Representative image of the sparse transduction of CA1 pyramidal cells by AAV1-
764 Cre:GFP counterstained by DAPI. Scale bar indicates 100μm. **(B)** Schematic of
765 experimental setup. Dual whole-cell EPSC recordings from Schaffer collateral
766 stimulation were made from neighboring transduced and control CA1 pyramidal cells.
767 **(C)** Scatterplot of paired neuronal recordings of P14-21 NMDAR-EPSCs (open circles)
768 and averaged pair ± SEM (solid circle). Sample trace bars indicate 200 ms, 30 pA.
769 Average NMDAR-EPSC amplitudes for control (131.7 ± 25.9 pA, n = 11) and Cre:GFP+
770 neurons (114.0 ± 24.4 pA, n = 11; t(10) = 1.625, p = 0.1351, ratio paired *t* test). **(D)**
771 Average decay kinetics of NMDAR-EPSCs for control (170.0 ± 7.5 ms, n = 10) and
772 Cre:GFP+ neurons (173.1 ± 10.8 ms, n = 10) from paired recordings in C (t(9) = 0.2197,
773 p = 0.8310, paired *t* test). **(E)** Scatterplot of paired neuronal recordings of P14-21
774 AMPAR-EPSCs (open circles) and averaged pair ± SEM (solid circle). Sample trace bars
775 indicate 200ms, 30pA. Average AMPAR-EPSC amplitudes for control (85.9 ± 22.3 pA; n
776 = 9) and Cre:GFP+ neurons (91.0 ± 20.2 pA; n = 9; t(8) = 0.7780, p = 0.4590, ratio

paired *t* test). **(F)** Average paired pulse ratio for control (2.21 ± 0.28, n = 4) and Cre:GFP+ neurons (1.94 ± 0.21, n = 4; t(6) = 0.7694, p = 0.4708, *t* test). Sample trace bars indicate 100 ms, 30 pA.

Figure 6: Reduced NMDAR-EPSCs at P45-70 following single-neuron SR deletion **(A)** Scatterplot of paired neuronal recordings of P45-70 NMDAR-EPSCs (open circles) and averaged pair ± SEM (solid circle). Sample trace bars indicate 200 ms, 30 pA. Average NMDAR-EPSC amplitudes for control (144.1 ± 18.9 pA, n = 19) and Cre:GFP+ neurons (87.6 ± 11.7 pA, n = 19; t(18) = 3.689, p = 0.0017, ratio paired *t* test). **(B)** Scatterplot of paired neuronal recordings of P45-70 AMPAR-EPSCs (open circles) and averaged pair ± SEM (solid circle). Sample trace bars indicate 200ms, 30pA. Average AMPAR-EPSC amplitudes for control (111.8 ± 19.0 pA, n = 14) and Cre:GFP+ neurons (85.4 ± 15.7 pA, n = 14; t(13) = 1.936, p = 0.0749, ratio paired *t* test). **(C)** Average paired pulse ratio for control (1.83 ± 0.15, n = 9) and Cre:GFP+ neurons (1.70 ± 0.22, n = 9; t(16) = 0.4649, p = 0.6483, *t* test). Sample trace bars indicate 100 ms, 30 pA. **(D)** Left, averaged whole-cell LTP experiments and representative traces (50 ms, 30 pA). Middle, summary of average percentage potentiation relative to baseline; control neurons (193.9 ± 22.1 %, n = 12), Cre:GFP+ neurons (196.6 ± 15.1 %, n = 12; t(22) = 0.09961, p = 0.9216, *t* test). Right, cumulative distribution of experiments.

Figure 7: Single-neuron SR deletion increases synaptic GluN2B **(A)** Averaged whole-cell D-serine wash experiments and representative traces (50ms, 30pA). Summary of average percentage potentiation relative to baseline; control neurons (125.6 ± 4.1 %, n = 14), Cre:GFP+ neurons (117.4 ± 14.4 %, n = 7; t(19) = 0.7147,

p = 0.4835, *t* test). Cumulative distribution of experiments. **(B)** Average decay kinetics of NMDAR-EPSCs for control (191.1 ± 12.1 ms, n = 19) and Cre:GFP+ neurons (288.6 ± 30.6 ms, n = 19) from paired recordings in Fig 6A (t(18) = 3.040, p = 0.0070, paired *t* test). **(C)** Averaged whole-cell R025 wash experiments and representative traces (200 ms, 50 pA). Summary of average percentage of current sensitive to R025 wash; control neurons (24.8 ± 8.7 %, n = 6), Cre:GFP+ neurons (61.2 ± 14.5 %, n = 4; t(8) = 2.340, p = 0.0474, *t* test). **(D)** Average charge transfer of NMDAR-EPSCs for control (40.2 ± 5.4 pC, n = 19) and Cre:GFP+ neurons (32.3 ± 3.9 pC, n = 19) from paired recordings in Fig 6A (t(18) = 1.518, p = 0.1464, paired *t* test).

Figure 8: Loss of LTP at P23-39 following single-neuron SR deletion

(A) Scatterplot of paired neuronal recordings of P23-39 NMDAR-EPSCs (open circles) and averaged pair ± SEM (solid circle). Sample trace bars indicate 200 ms, 30 pA. Average NMDAR-EPSC amplitudes for control (91.7 ± 27.7 pA, n = 9) and Cre:GFP+ neurons (140.8 ± 26.3 pA; t(8) = 1.879, p = 0.0970, ratio paired *t* test). **(B)** Average decay kinetics of NMDAR-EPSCs for control (200.8 ± 19.4 ms, n = 7) and Cre:GFP+ neurons (268.3 ± 60.4 ms, n = 7) from paired recordings in A (t(6) = 1.510, p = 0.1818, paired *t* test). **(C)** Scatterplot of paired neuronal recordings of P23-39 AMPAR-EPSCs (open circles) and averaged pair ± SEM (solid circle). Sample trace bars indicate 200 ms, 30 pA. Average AMPAR-EPSC amplitudes for control (60.8 ± 12.7 pA, n =11) and Cre:GFP+ neurons (73.4 ± 10.4 pA, n = 11 ; t(10) = 1.724, p = 0.1155, ratio paired *t* test). **(D)** Average paired pulse ratio for control (2.06 ± 0.21, n = 5) and Cre:GFP+ neurons (2.05 ± 0.12; t(8) = 0.01663, p = 0.9871, *t* test). Sample trace bars indicate 100 ms, 30 pA. **(E)** Left, averaged whole-cell LTP experiments and representative traces of control

neurons (black), Cre:GFP+ neurons (blue), and Cre:GFP+ neurons with 100 μM exogenous D-serine administered through the end of the induction (red) (50 ms, 30 pA). Middle, summary of average percentage potentiation relative to baseline; control neurons (151.9 ± 10.3 %, n = 8), Cre:GFP+ neurons (100.2 ± 6.1 %, n = 6; $t(12) = 3.955$, $p = 0.0019$, *t* test) , Cre:GFP+ neurons with 100μM D-serine (164.8 ± 15.3 %, n = 8; $t(14) = 0.7032$, $p = 0.4934$, *t* test). Right, cumulative distribution of experiments.

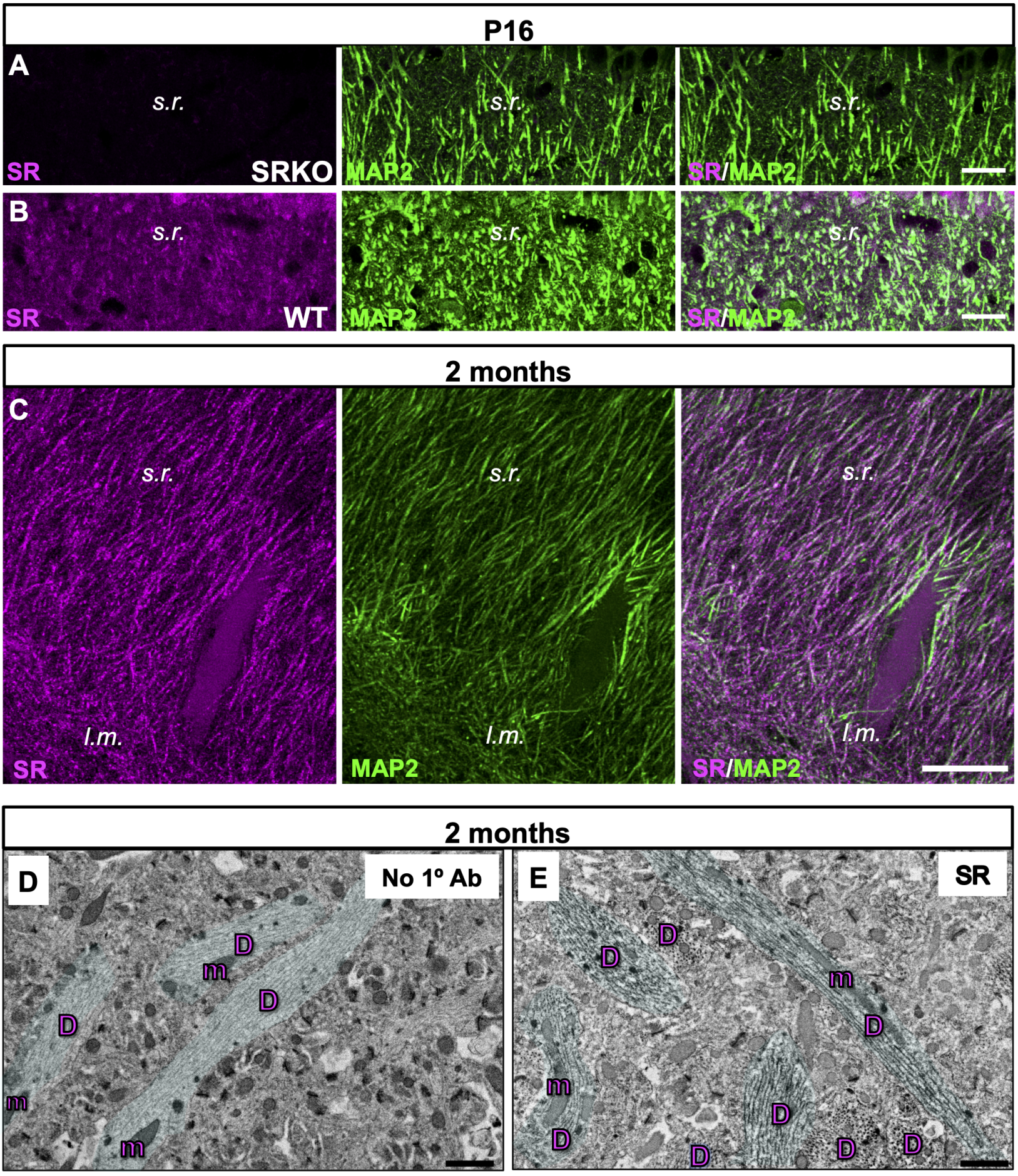
P16
A
s.r.
SR
SRKO
s.r.
MAP2
s.r.
SR/MAP2
B
s.r.
SR
WT
s.r.
MAP2
s.r.
SR/MAP2
2 months
C
s.r.
l.m.
SR
s.r.
l.m.
MAP2
s.r.
l.m.
SR/MAP2
2 months
D
No 1º Ab
D
m
D
D
m
m
E
SR
D
D
m
D
m
D
D
D
D
D

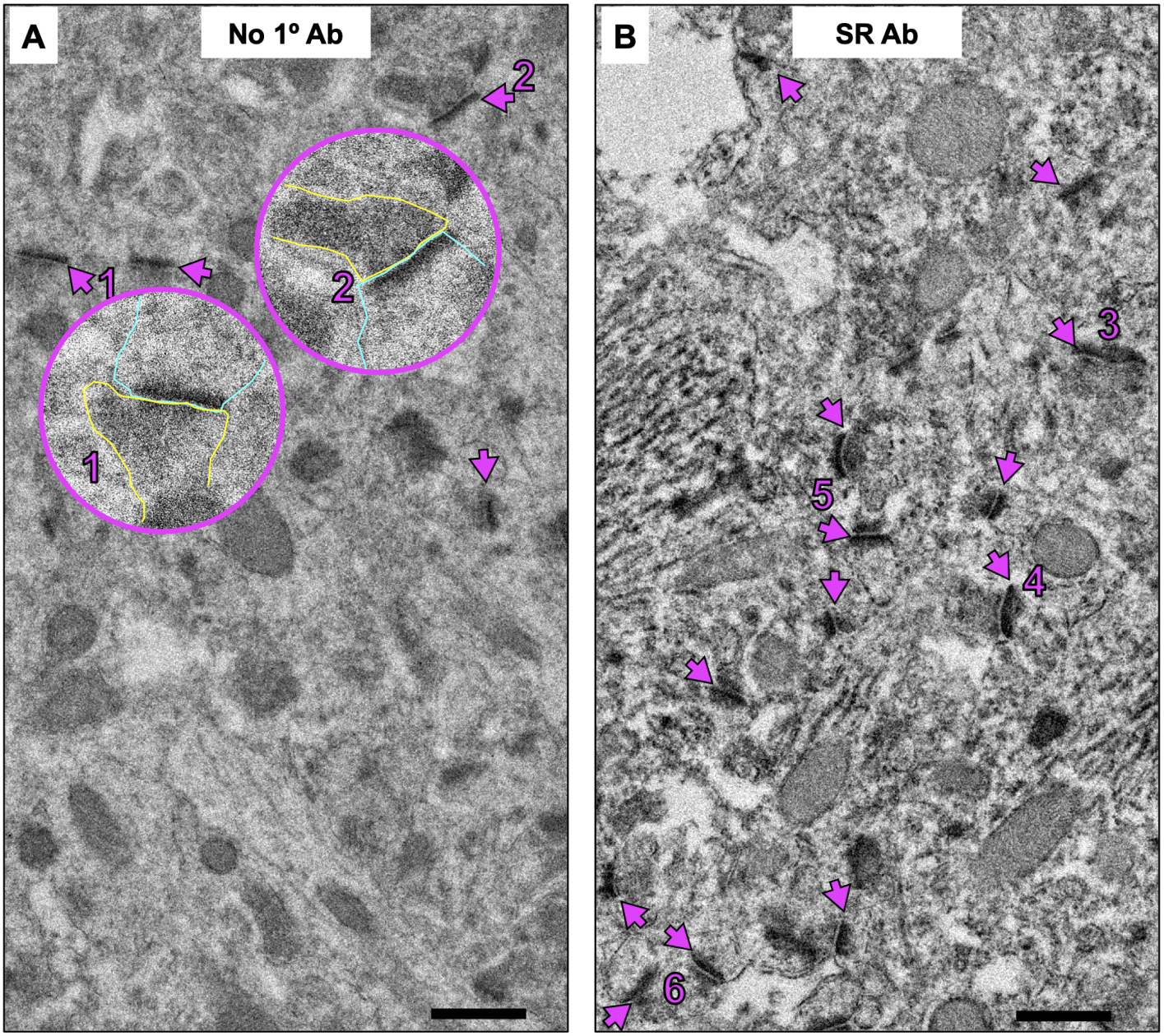
A
No 1º Ab
1
2
B
SR Ab
3
4
5
6

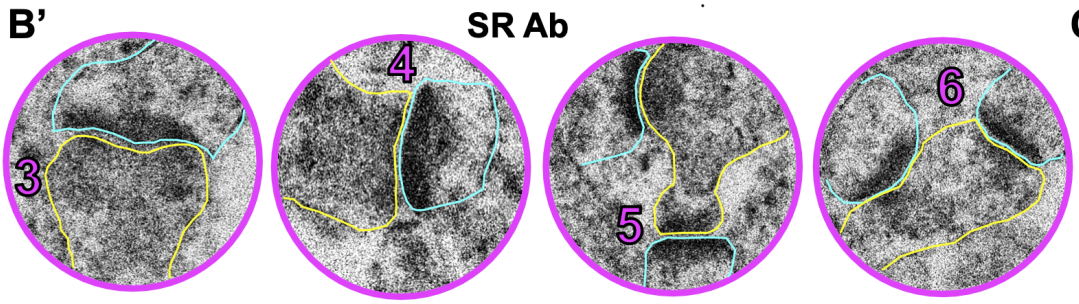
B'
SR Ab
3
4
5
6

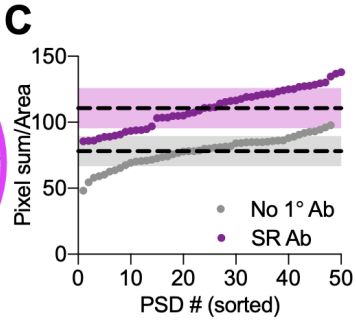
C
150
100
50
0
Pixel sum/Area
No 1° Ab
SR Ab
0
10
20
30
40
50
PSD # (sorted)

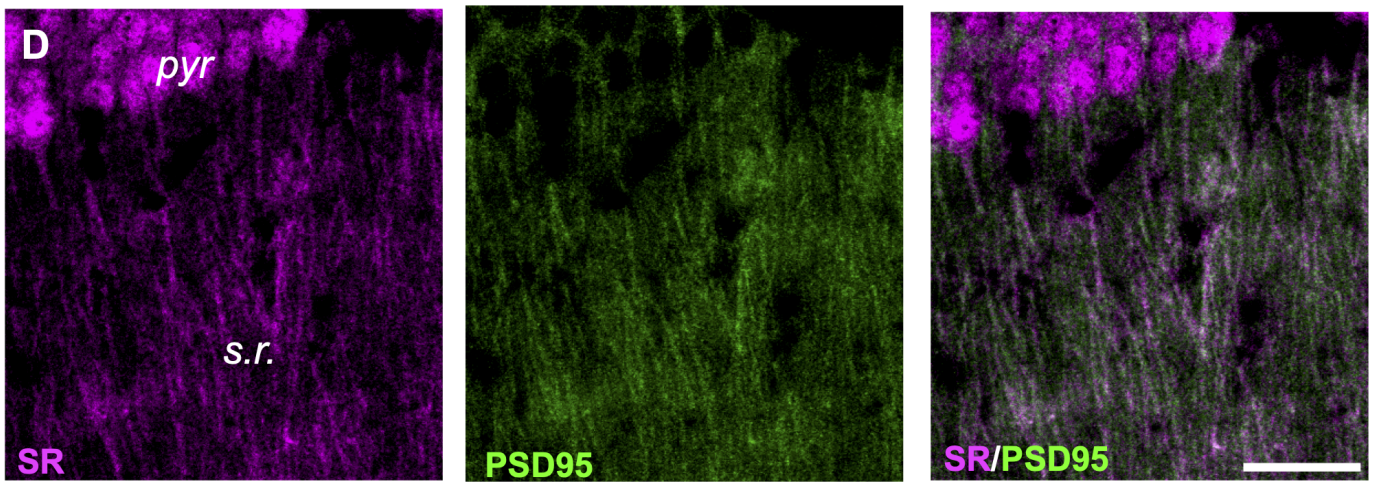
D
pyr
s.r.
SR
PSD95
SR/PSD95

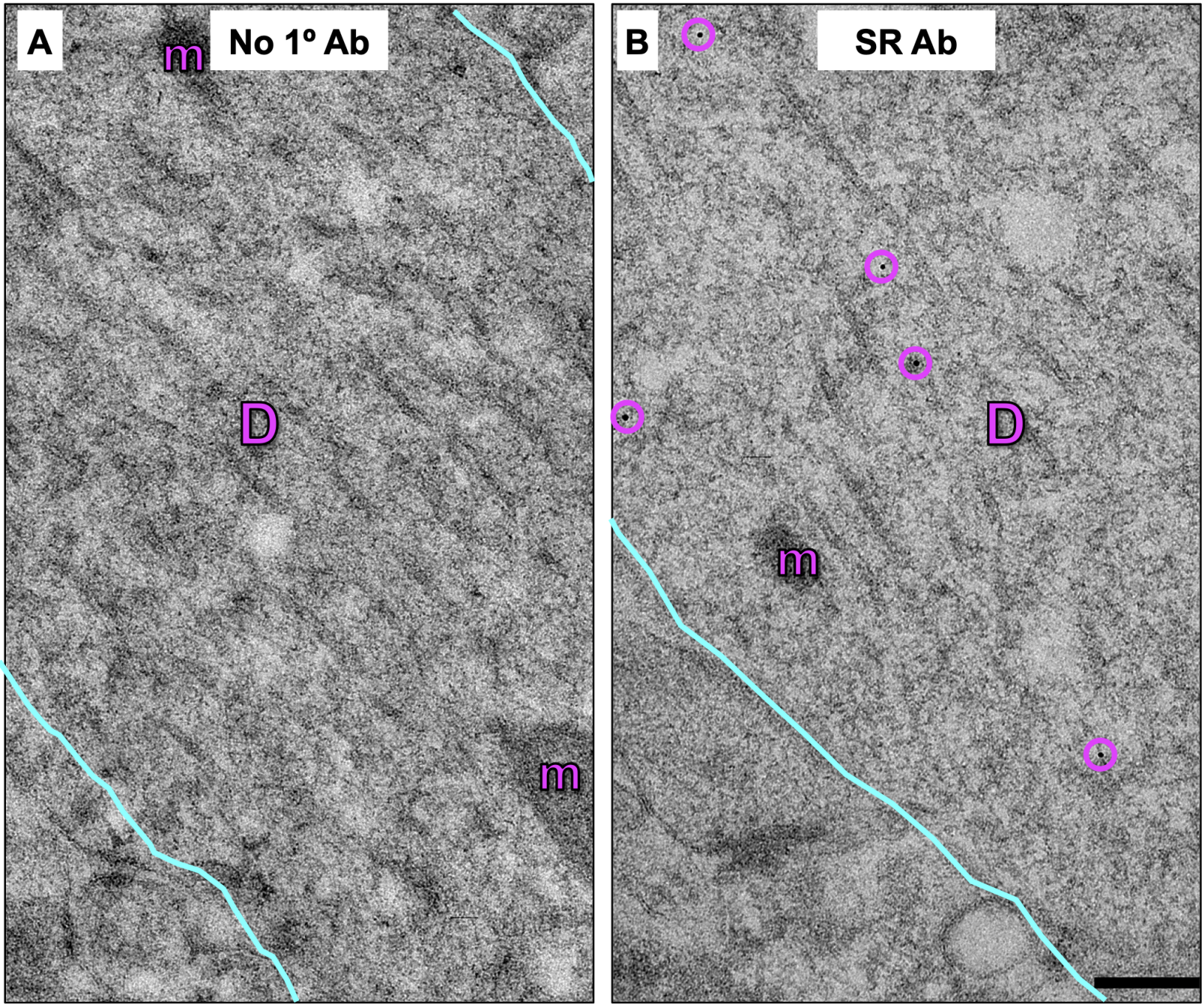
A
No 1° Ab
m
D
m
B
SR Ab
D
m

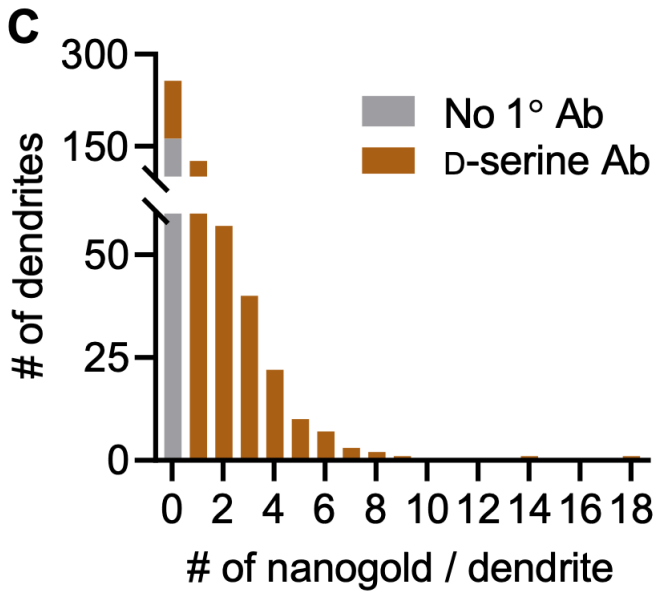
C
300
150
50
25
0
# of dendrites
No 1° Ab
D-serine Ab
0 2 4 6 8 10 12 14 16 18
# of nanogold / dendrite

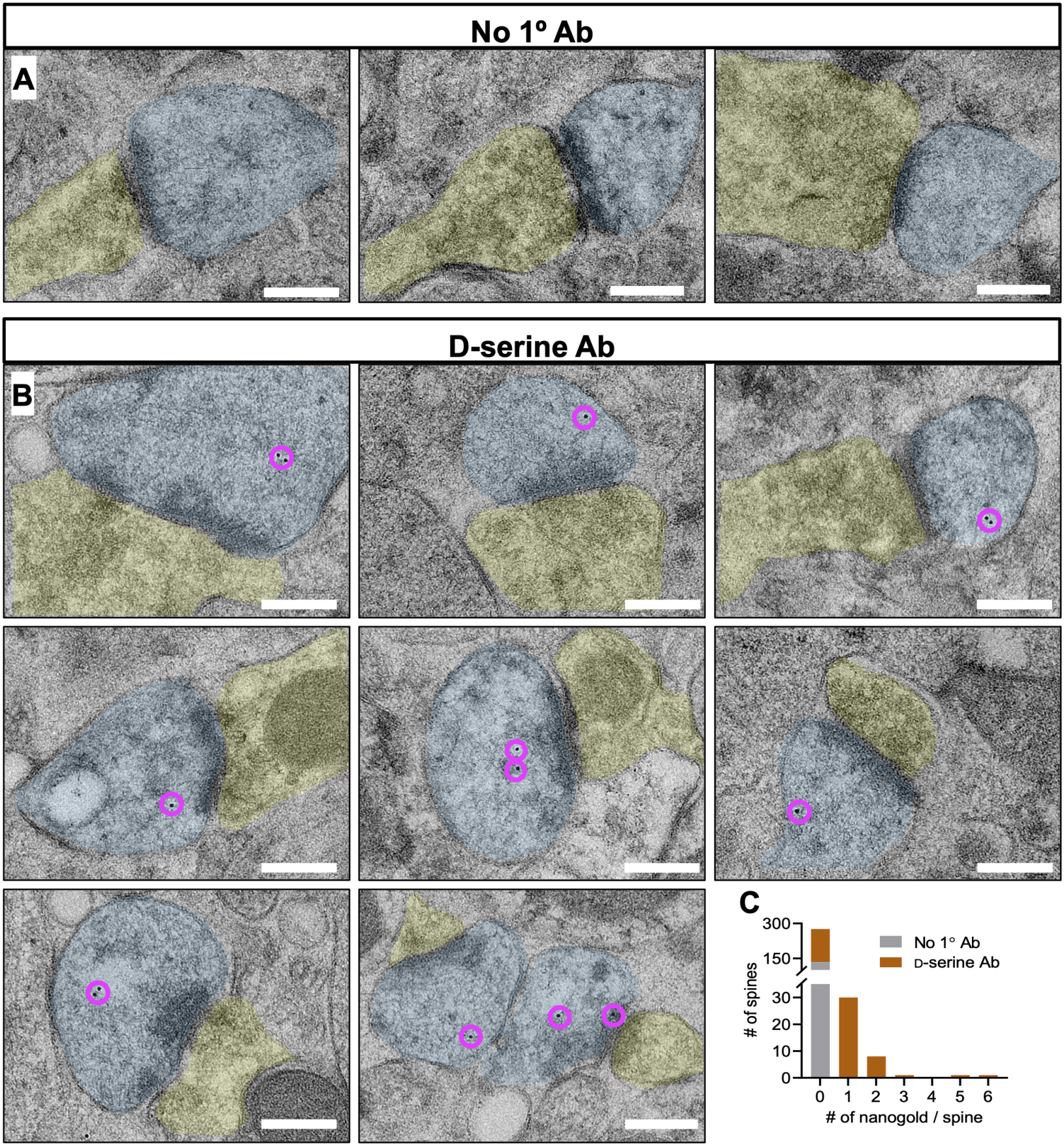
No 1º Ab
A
D-serine Ab
B
C
300
150
30
20
10
0
# of spines
No 1° Ab
D-serine Ab
0 1 2 3 4 5 6
# of nanogold / spine

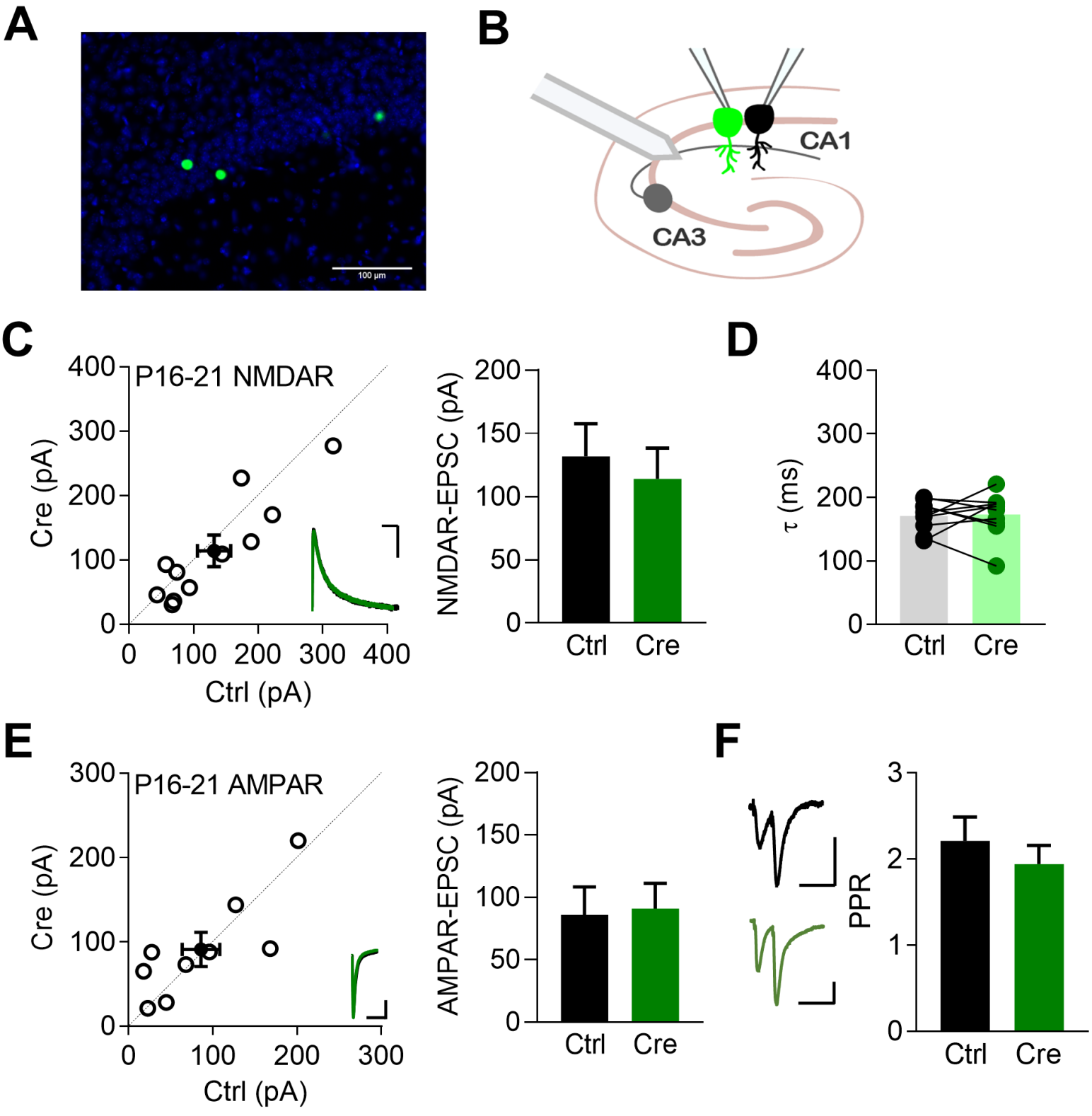
A
100 µm
B
CA1
CA3
C
P16-21 NMDAR
Cre (pA)
Ctrl (pA)
0
100
200
300
400
NMDAR-EPSC (pA)
150
50
Ctrl
Cre
D
τ (ms)
E
P16-21 AMPAR
AMPAR-EPSC (pA)
F
PPR
1
2
3

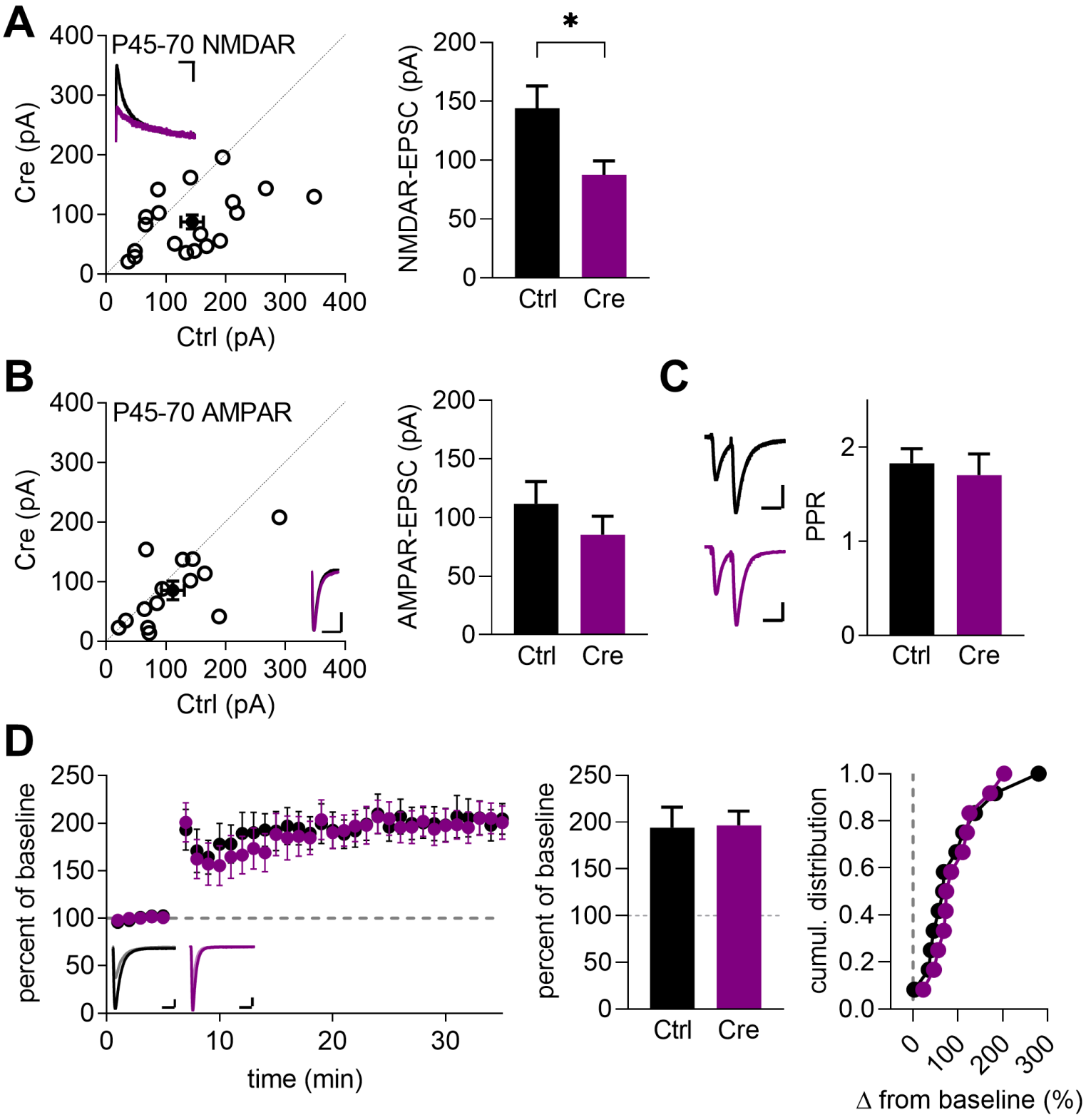
A
P45-70 NMDAR
Cre (pA)
Ctrl (pA)
0
100
200
300
400
NMDAR-EPSC (pA)
*
Ctrl
Cre
B
P45-70 AMPAR
AMPAR-EPSC (pA)
C
PPR
D
percent of baseline
time (min)
cumul. distribution
Δ from baseline (%)

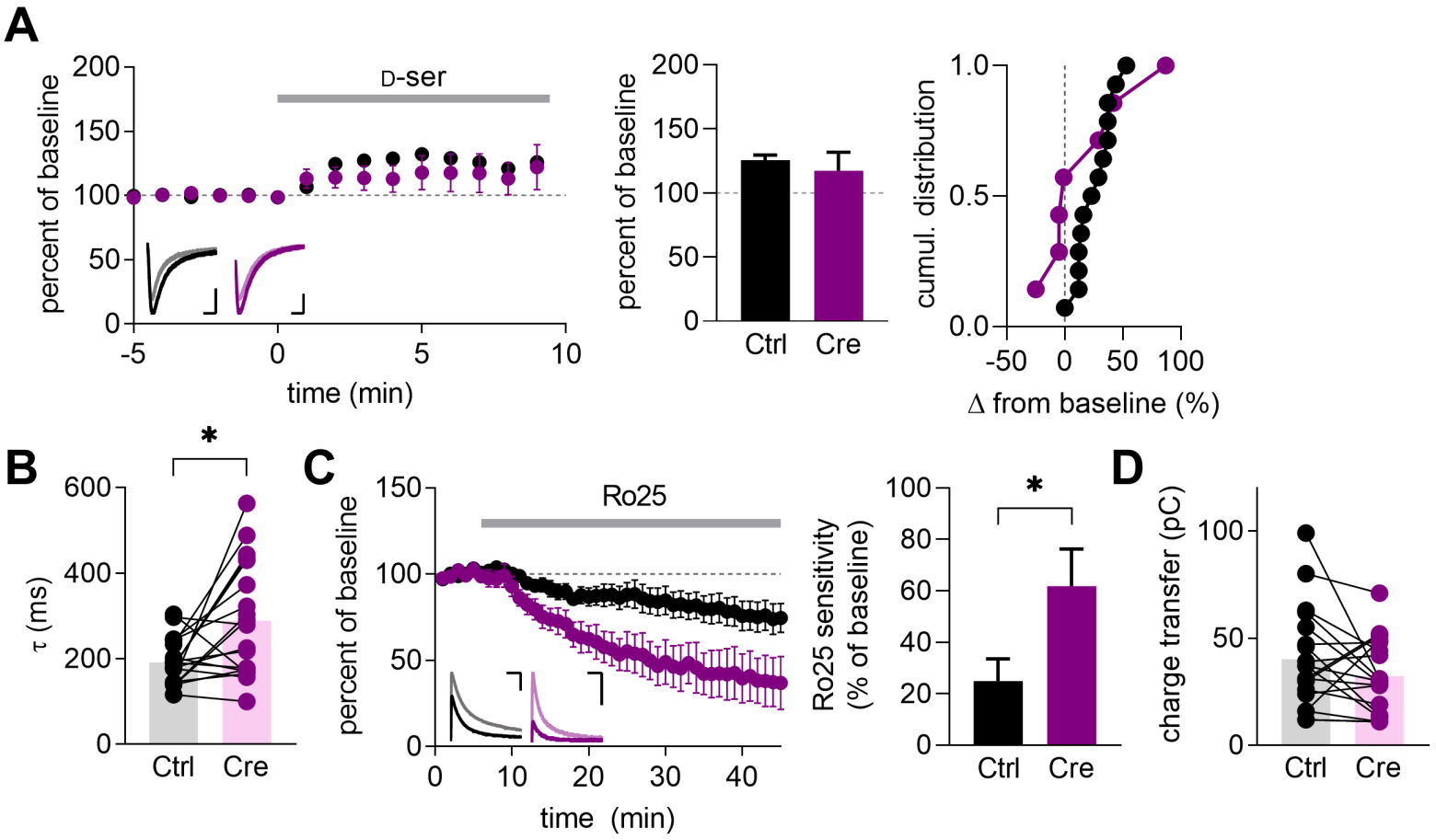
A
D-ser
percent of baseline
time (min)
Ctrl
Cre
cumul. distribution
Δ from baseline (%)
B
τ (ms)
*
C
Ro25
percent of baseline
time (min)
Ro25 sensitivity (% of baseline)
D
charge transfer (pC)

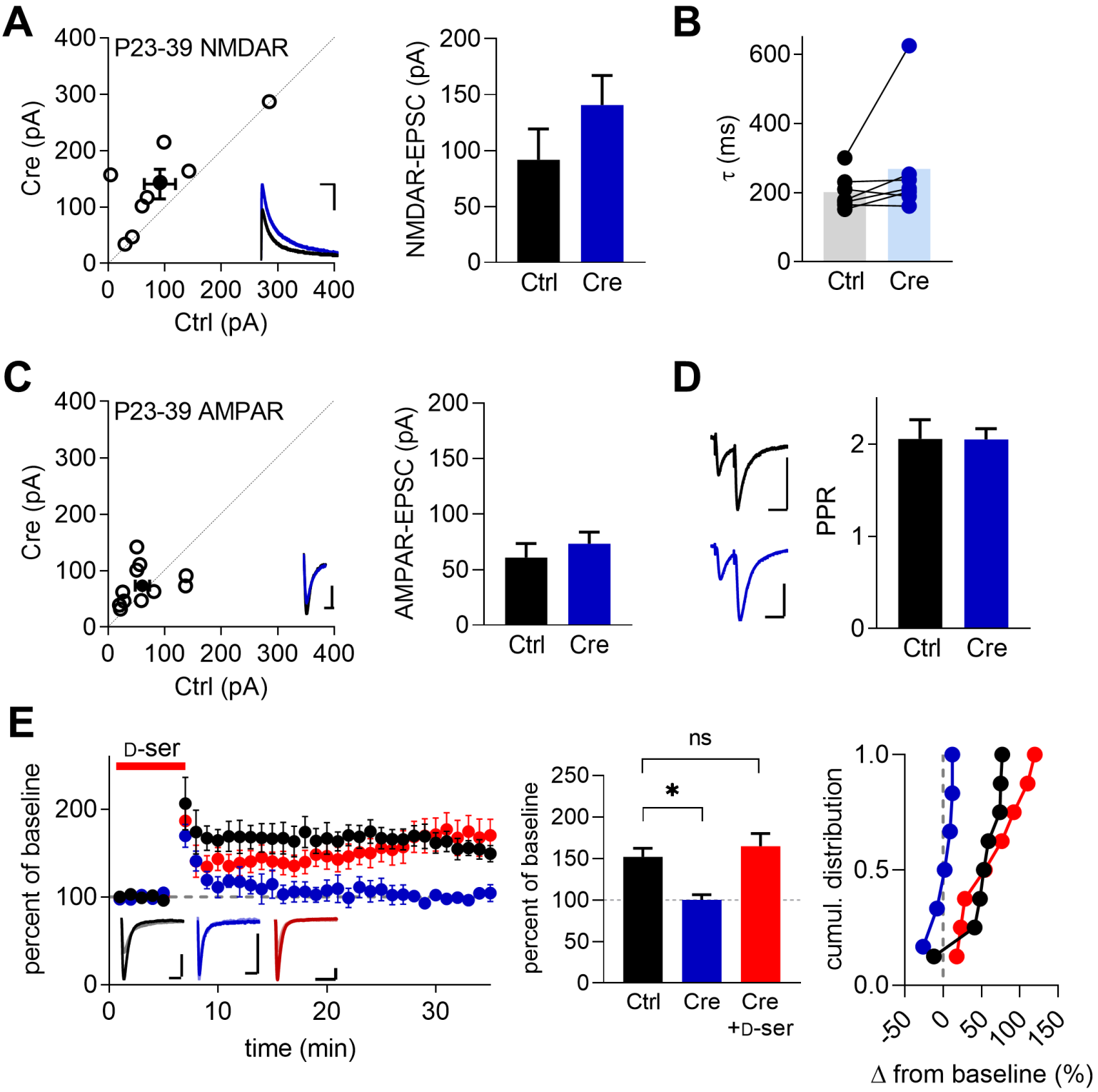
A
P23-39 NMDAR
Cre (pA)
Ctrl (pA)
0
100
200
300
400
NMDAR-EPSC (pA)
50
150
Ctrl
Cre
B
τ (ms)
600
C
P23-39 AMPAR
AMPAR-EPSC (pA)
D
PPR
1
2
E
D-ser
percent of baseline
time (min)
ns
*
+D-ser
cumul. distribution
Δ from baseline (%)
-50
0.0
0.5
1.0